OPTICAL PROPERTIES OF MATERIALS AT LOW TEMPERATURE AND THEIR APPLICATION TO OPTICAL DETECTION

FINAL REPORT

GRANT NGR 44-012-104

NATIONAL AERONAUTICS AND SPACE ADMINISTRATION

August 31, 1972

by

William H. Hartwig

and Andrea Albanese Tarchi

Department of Electrical Engineering

THE UNIVERSITY OF TEXAS AT AUSTIN

Austin, Texas 78712

PREFACE

This Final Report completes a research project, initiated in June 1968, to examine the photodielectric effect in semiconductors as the basis for a new optical detector. The work was stimulated by the need for better detectors of optical radiation at all wavelengths. The observation of the photodielectric effect in 1966 by the author and his students demonstrated the feasibility of a detector consisting of an illuminated semiconductor wafer in a microwave cavity causing a resonant frequency shift proportional to light intensity. The first published paper appeared in the May, 1968 issue of the Journal of Applied Physics (Ref. 3 in this report).

The proposal to NASA was for support of a basic research study on semiconductors at low temperatures to discover the nature of their optical response, particularly with respect to sensitivity, bandwidth and wavelength. The grant has supported an investigation of several semiconductors with different energy gaps, corresponding to several different wavelengths. The photodielectric detector can be made to have its peak response at any wavelength for which a semiconductor can be found with a suitable optical transition. In each case the free carriers generated produce a change in crystal polarization by virtue of their dynamic response to the RF electric field in the crystal. A typical example is a sensitivity of several hundred KHz change in the frequency of a 1 GHz resonator with a silicon wafer illuminated with GaAs diode light at about 1 mW/cm^2 at 4.2°K. The active volume of the sample is controlled by the photon penetration depth into the wafer, which depends upon the relative photon energy compared to the bandgap.

In the course of this research the photodielectric effect has shown itself to be a powerful technique to study the optical and thermal

response of various materials as well as the defect structure of single crystals. Work on III-V and II-VI compounds (Ref. 2) showed the photodielectric effect could be used to study the trapping and recombination dynamics of semiconductor crystals and powders. The principal advantages include the absence of need for ohmic contacts, the absence of such contact effects as contamination and rectification, and the ability to use powder samples.

The derivation of an appropriate figure of merit was recognized as one of the most important problems posed by a detector user, since his acceptance of a new detector must, ultimately, be based upon system design consideration. These would include a critical comparison of all detectors. Unfortunately, the photodielectric detector produces a frequency shift in response to a change in light intensity, whereas more conventional bulk and junction photodetectors produce voltage changes. This report addresses itself to reconciling that problem.

The sensitivity, in Hz/watt, is readily measurable and is clearly a function of many cavity and sample parameters. No simple answer could be found to the question of detector bandwidth, since the cavity Q, carrier lifetime and external circuit all play a part. This report defines the problem and undertakes a closed-form solution for the case of low Q.

The present work is an analysis of the free-carrier photodielectric effect (PDE) used for optical and infrared detection. The main goal is to compare detectors utilizing the PDE with other detectors already known, to define useful parameters, and to determine the advantages and limitations of such detectors.

The analysis is divided into three parts:

FIRST. The study of interactions between the microwave fields and the semiconductor sample is required to define the PDE. Different models are developed to represent different types of semiconductors (samples) and also to simplify the subsequent analysis.

SECOND. The study of a system to measure the PDE continuously is undertaken to find the noise sources and conditions which limit the performance of the PDE detector.

THIRD. The study is extended to the interaction between the radiation to be detected and the sample used as detector. The literature on the photodielectric effect and on photoconductors is used to compare the PDE of different materials with more familiar detectors.

This report is largely the work of Andrea Albanese, who studied the previous work by the senior author and his collaborators, and offered the analysis as his M.S. thesis.

ABSTRACT

A lumped model to represent the photodielectric effect is developed. An analog simulation for a sample in a microwave cavity with a static magnetic field is developed. A system to measure continuously the PDE is analyzed. A performance factor to compare PD detectors versus AC photoconductors is computed. The operating conditions are defined for the appropriate noise conditions. The detectivity of the detector is found to be limited by the semiconductor sample noise.

TABLE OF CONTENTS

LIST OF FIGURES

CHAPTER I.

A CIRCUIT MODEL TO REPRESENT THE PHOTODIELECTRIC EFFECT

1. INTRODUCTION

We define a circuit model which allows us to describe the properties of a given sample (semiconductor) in a parametric way. A lumped model is developed because it has the following advantages:

FIRST. It facilitates the understanding of the PDE's properties when it is used as a detector of infrared or optical radiation.

SECOND. It allows us to define parameters such as Q, bandwidth B_W, resistance R_s, inductance L_s, and capacitance C_o of the sample. In turn, these parameters make it easier to calculate quantities such as energy stored and dissipated by the sample and also the noise produced by the sample.

THIRD. Finally, the circuit representation of the lumped model allows us to compare the PDE with other known mechanisms used in detectors which also have a circuit representation.

2. THE PHOTODIELECTRIC EFFECT

The PDE is explained by analysis of the equation of motion for the electrons within the semiconductor, assuming hole effects are analogous and smaller. We separate the dielectric constant into two contributions that are due to bound carriers and to free carriers. The bound electrons account for the lattice dielectric constant, K_ℓ. The free electrons also produce a contribution to the total dielectric constant K due to their inertial forces in an AC field, as given by Dresselhaus, Kip and Kittel[4] and by Michel and Rosenblum[5]. Effects of trapped electrons, as described by Hinds and Hartwig[2] are not included.

All the contributions could be computed, assuming that the electrons behave like a damped oscillator, and this is related by

$$K = 1 + \kappa_b + \kappa_f \qquad [1]$$

where K = the total dielectric constant,

κ_b = the susceptibility of the bound carriers in MKS units, and

κ_f = the susceptibility of the free carriers.

The equation of motion of the free carriers is:

$$eE_x = m^*\ddot{x} + m^*\frac{\dot{x}}{\tau} + m^*\omega_p^2 x \qquad [2]$$

where m^* = the effective mass,

τ = the relaxation time,

ω_p = the plasma frequency, and

E_x = the macroscopic electric field.

To that:

eE_x = the total external force that acts on the electron,

$m^*\ddot{x}$ = the inertial force of the electron,

$m^*\frac{\dot{x}}{\tau}$ = the friction force, due to collisions and scattering of the electrons, and

$m^*\omega_p^2 x$ = the restoring force which ties the electron to the sample.

In free electrons, this is due to space charge or Coulomb interaction between electrons and the lattice. In the case of bound charges, it is called $m^*\omega_o^2 x_b$, which is due to the Coulomb interaction between the nucleus and the electron. In both cases, the restoring forces are manifested by the depolarization field P which appears when we applied a constant electric field E to the sample[6].

Figure 1 shows a sample with free charges to which is applied an electric field E which causes the charges to separate according to charge

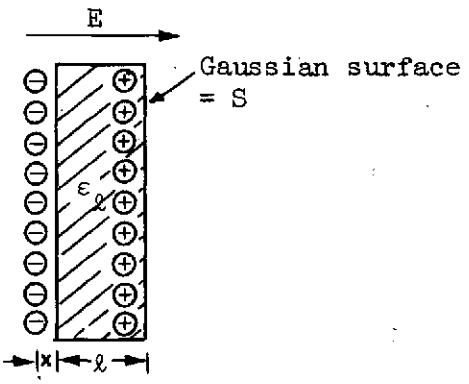

FIGURE 1. Model to compute the electron restoring force in the semiconductor when an external electric field E is applied.

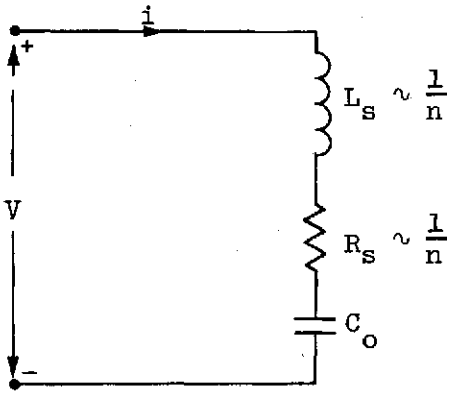

FIGURE 2. Equivalent circuit for the free electrons into a semiconductor.

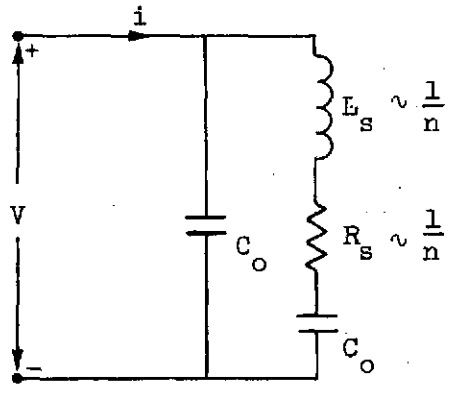

FIGURE 3. Equivalent circuit for the electrons and the lattice.

polarity. This bipolar separation may be represented by the formation of an electric dipole moment originating from the displacement of charge carriers from their average position. The restoring field is

$$E_r = \frac{Q}{S\varepsilon_\ell} = \frac{nex}{\varepsilon_\ell} \qquad [3]$$

which is computed applying the Gauss' law. The ratio Q/S is the electron surface density, ε_ℓ is the lattice permittivity, n is the electron density, e is the electron charge, and x is the average distance displaced.

From Eq. [3] the electron restoring force is

$$F_r = eE_r = \frac{ne^2x}{\varepsilon_\ell} = m^*\omega_p^2 x \qquad [4]$$

for

$$\omega_p^2 = \frac{ne^2}{m^*\varepsilon_\ell}. \qquad [5]$$

Note that Figure 1 shows a rectangular slab which implies a depolarization factor[7] L = 1.

The conduction current is defined as

$$i = neA\dot{x} \qquad [6]$$

which implies

$$\dot{x} = \frac{1}{neA}\, i$$

$$x = \frac{1}{neA} \int i\,dt \qquad [7]$$

$$\ddot{x} = \frac{1}{neA}\, \dot{i}.$$

The dot denotes the time derivative.

Replacing the variables of Eq. [7] into the equation of motion [2], and multiplying both sides by the length of the sample along the applied electric field we get:

$$V = \frac{m^*\ell}{ne^2A}\dot{i} + \frac{m^*\ell}{ne^2A\tau} i + \frac{m^*\ell}{ne^2A}\omega_p^2 \int i\,dt \qquad [8]$$

where $V = E_x \cdot \ell$.

Eq. [8] can be written as

$$V = L_s \frac{di}{dt} + R_s i + \frac{1}{C_o} \int i\,dt \qquad [9]$$

where

$$R_s = \frac{m^*\ell}{ne^2A} \qquad [10]$$

$$L_s \quad \frac{m^*\ell}{ne^2A\tau} \qquad [11]$$

$$C_o = \frac{\epsilon_\ell A}{\ell}. \qquad [12]$$

According to Eq. [9], the equation of motion for the free electrons can be represented with the circuit model shown in Figure 2.

A similar analysis may be made for the equation of motion of the bound carriers which cause the lattice dielectric constant. Knowing from the experiment[8] that the resonant frequency of the bound carriers is larger than the plasma frequency, then at frequencies near and below the plasma frequency the lattice contribution can be represented by a capacitor C_o in shunt to the circuit of Figure 2. The final model looks like the circuit represented by Figure 3.

The admittance $Y(\omega)$ of the latter circuit is written as

$$Y(\omega) = j\omega C_o \left[1 + \frac{\frac{1}{L_s C_o}}{\frac{1}{L_s C_o} - \omega^2 + j\omega\frac{R_s}{L_s}}\right]. \qquad [13]$$

With Eqs. [10], [11], [13], and [5] into Eq. [13], we have

$$Y(\omega) = j\omega \frac{A\epsilon_\ell}{\ell}\left[1 + \frac{\omega_p^2}{\omega_p^2 - \omega^2 + j\frac{\omega}{\tau}}\right] \qquad [14]$$

where the factor

$$\varepsilon_\ell \left[1 + \frac{\omega_p^2}{\omega_p^2 - \omega^2 + j\frac{\omega}{\tau}} \right] = \varepsilon(\omega)$$

is defined as the complex permittivity[9], and it was used in previous publications[1,2,3] to explain the PDE.

Figure 4 shows a modification of Figure 3 for the case when the sample has ohmic contacts. These eliminate the space charge which produces the restoring force and is represented by the series capacitor C_o. At low frequencies near DC Figure 4 reduces to Figure 5, which represents the known electrical model for photoconductors[10].

3. PHOTODIELECTRIC RESPONSE IN A STATIC MAGNETIC FIELD

The free carrier photodielectric theory has been derived above, and by others[3,4] for the case where the dynamic effects of electrons dominate over that of holes, and where there is only an RF electric field present. Since it is a straightforward matter to include a static magnetic field, this is done below to bring out new effects which have not been considered previously for the case of PDE.

The total electromagnetic force acting upon an electron is expressed by the Lorentz force:

$$-e[\bar{E} + \dot{\bar{r}} \times \bar{B}] = \overleftrightarrow{m^*}\ddot{\bar{r}} + \frac{\overleftrightarrow{m^*}}{\tau}\dot{\bar{r}} + \overleftrightarrow{m^*}\overleftrightarrow{\omega_p^2}\,\bar{r} \qquad [15]$$

and considering the case when $E = E_x$ and $B = B_z$, then $\dot{\bar{r}} \times \bar{B} = r_y B_z \hat{i} - r_x B_z \hat{j}$, and Eq. [15] can be written as

$$\ddot{r}_x + \frac{1}{\tau}\dot{r}_x + \omega_{p1}^2 r_x = -\frac{e}{m_1^*}E - \frac{eB_z}{m_1^*}\dot{r}_y$$

$$\ddot{r}_y + \frac{1}{\tau}\dot{r}_y + \omega_{p2}^2 r_y = \frac{eB_z}{m_2^*}\dot{r}_x \qquad [15a]$$

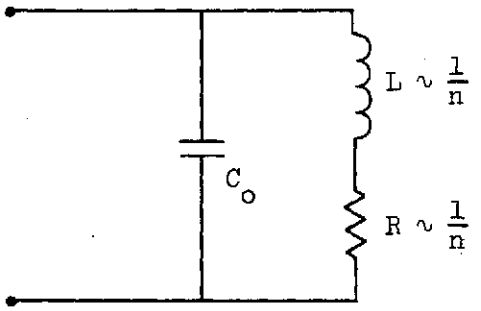

FIGURE 4. Equivalent circuit for the sample with ohmic contact.

The models permit a direct comparison between the AC photoconductive detector and photodielectric detector where there are no ohmic contacts to the sample.

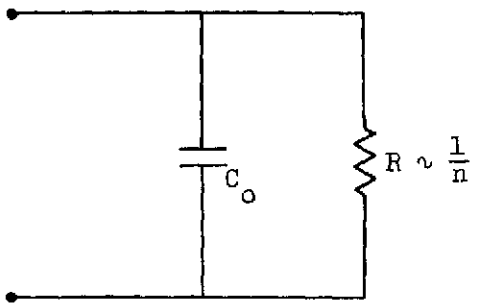

FIGURE 5. Equivalent circuit for a photoconductor.

For the case where ohmic contacts are made to a photoconductive detector, the frequency must be sufficiently high so the free carrier excursion in one-half cycle is less than the sample thickness.

calling $r_x = x$, $r_y = y$

$\dot{r}_x = v_x$, $\dot{r}_y = v_y$ and $\frac{eB_z}{m_i^*} = \omega_{ci}$

we can express Eq. [15a] in the state form:

$$\begin{bmatrix} \dot{x} \\ \dot{v}_x \\ \dot{y} \\ \dot{v}_y \end{bmatrix} = \begin{bmatrix} 0 & 1 & 0 & 0 \\ -\omega_{p1}^2 & -\frac{1}{\tau} & 0 & -\omega_{c1} \\ 0 & 0 & 0 & 1 \\ 0 & \omega_{c2} & -\omega_{p2}^2 & -\frac{1}{\tau} \end{bmatrix} x \begin{bmatrix} x \\ v_x \\ y \\ v_y \end{bmatrix} + \begin{bmatrix} 0 \\ -\frac{e}{m_1^*} \\ 0 \\ 0 \end{bmatrix} E \qquad [16]$$

which, without magnetic field, Eq. [16] reduces to the case treated in Section II:

$$\begin{bmatrix} \dot{x} \\ \dot{v}_x \end{bmatrix} = \begin{bmatrix} 0 & 1 \\ -\omega_{p1}^2 & -\frac{1}{\tau} \end{bmatrix} \begin{bmatrix} x \\ v_x \end{bmatrix} + \begin{bmatrix} 0 \\ -\frac{e}{m_1^*} \end{bmatrix} E \qquad [17]$$

The expression for v_x is found by solving Eq. [16], and the sample density current is $j = nev_x$.

Two more general cases which include (1) electron and hole dynamic effects with a static B-field; and (2) free, bound and trapped electron dynamics in an E field are too complex for a single comparison with the experiment. The equation for these cases, corresponding to Eq. [16] above, are given in Appendices A and B for completeness.

4. CIRCUIT REPRESENTATION OF THE CAVITY[11]

A cavity can be represented by a lumped equivalent circuit (Figure 6), which is a good approximation for behavior at frequencies near the cavity resonant frequency (or single mode).

In Figure 6, jX is the reactive effect of the modes far from resonance and G, L, C represents the mode near resonance.

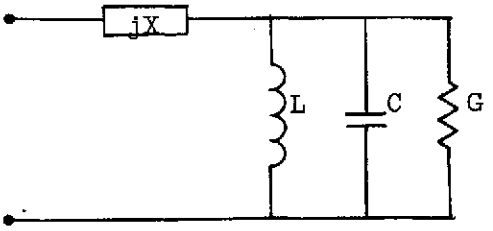

FIGURE 6. Equivalent circuit of a microwave cavity mode.

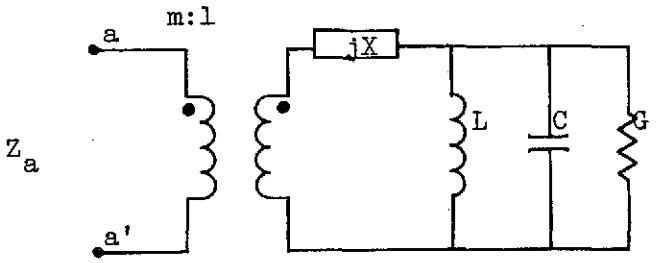

FIGURE 7. Equivalent circuit of the microwave cavity coupled to a waveguide.

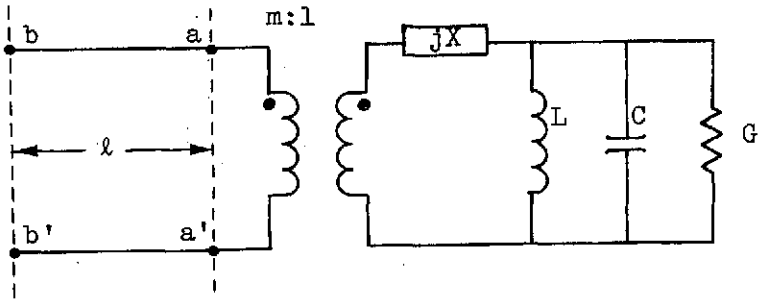

FIGURE 8. Equivalent circuit of the microwave cavity matched to the waveguide.

When the cavity is coupled to a waveguide this can be represented by the ideal transformer of turns ratio m:1 (Figure 7), where m is the voltage coupling transfer ratio.

Some relations for the cavity without a sample are:

$$Z_a = m^2\left[jX + \frac{1}{G + j(\omega C - \frac{1}{\omega L})}\right] = \text{input impedance.}$$

Defining

$$Q_o = \frac{\omega_o C}{G},\ \omega_o^2 = \frac{1}{LC} \text{ and } R = \frac{1}{G},$$

Z_a can be approximated by

$$Z_a \simeq jm^2X + \frac{m^2R}{1 + j2Q\delta'} \qquad [18]$$

where

$$\delta' = \frac{\omega - \omega_o}{\omega_o}.$$

The series reactance jX can be removed either by defining a new resonant frequency or by referring the input to a shifted point on the waveguide. The latter is a common and a new reference may be taken as the position of the "detuned short." That is, the cavity is detuned enough to make $Q_o\delta' >> 1$, either by detuning the cavity itself (changing ω_o) or changing the frequency ω.

By Eq. [18] the termination is then essentially jm^2X and the "detuned short" will be at the position ℓ from the end where $R_o \tan \beta\ell = m^2X$ Then from Figure 8 the impedance at the point b is

$$Z_b = \frac{Z_a + jR_o \tan \beta\ell}{1 + j(Z_a/R_o)\tan \beta\ell} = \frac{m^2R_b}{1 + j2Q_o\delta} \qquad [19]$$

where $R_b = R(1 + m^4x^2)^{-1}$

and $\delta = \delta' - \frac{m^4XR_b}{2Q_o}$

or

$$\delta = \frac{\omega - \omega_o(1 + m^4 X R_b/2Q_o)}{\omega_o}$$

where

$$\omega_r = \omega_o(1 + m^4 X R_b/2Q_o).$$

The reflection coefficient ρ at point b is

$$\rho = \frac{V_-}{V_+} = \frac{Z_L - 1}{Z_L + 1} \qquad [20]$$

where $Z_L = Z_b/R_o$, and R_o is the characteristic impedance of the waveguide.

Inserting Eq. [19] into [20] yields

$$\rho = \frac{\frac{m^2 R_b}{R_o} - 1 - j2Q_o\delta}{\frac{m^2 R_b}{R_o} + 1 + j2Q_o\delta} \qquad [21]$$

and for critical coupling,

$$\frac{m^2 R_b}{R_o} = 1$$

we find

$$\rho_{cr} = \frac{jQ_o\delta}{1 + jQ_o\delta}. \qquad [22]$$

Note that ρ approaches to zero at the resonant frequency, and this fact is used to determine the resonant frequency of the cavity. The error sources in determining ρ are treated in Chapter III.

The insertion of a sample into the cavity may be represented by another ideal transformer of turns ratio 1:g, which connects the sample to the cavity (Figure 9), where g is related to the "filling" factor of the sample, n, as shown below in Eq. [30].

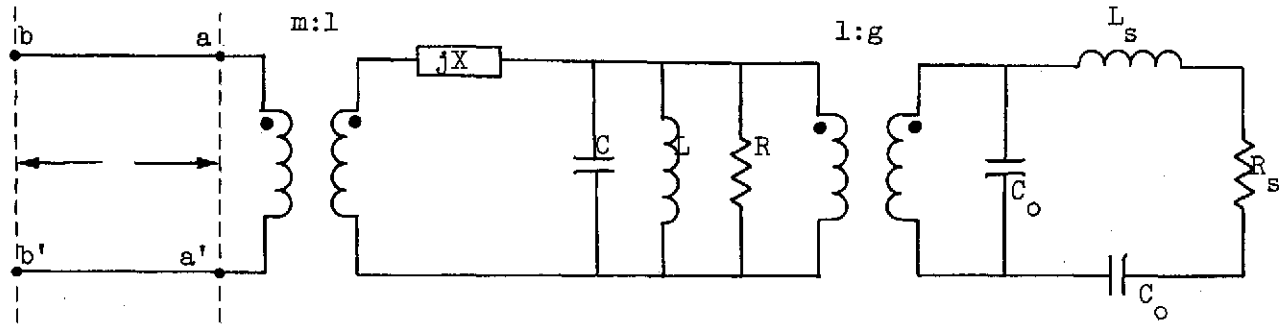

FIGURE 9. Equivalent circuit for a microwave cavity loaded with a sample (PDE).

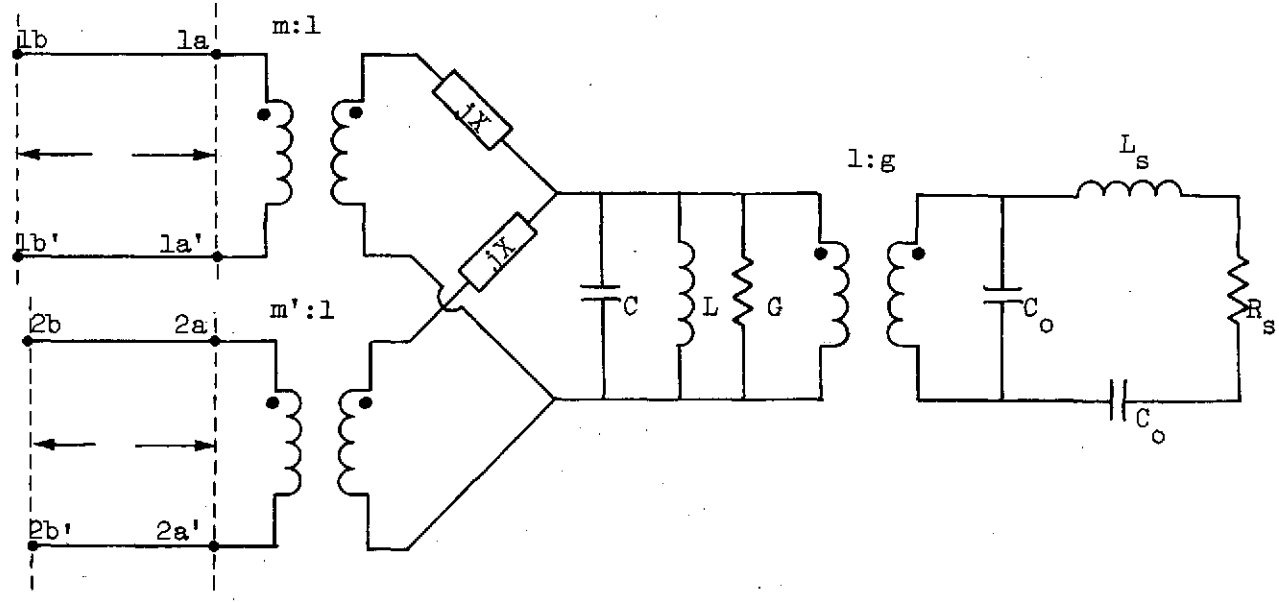

FIGURE 10. Equivalent circuit for a two-port microwave cavity loaded with a sample (PDE).

In general, a model for a two-port cavity and the sample is shown in Figure 10. This model would be used for a transmission cavity.

5. COMPLETE MODEL: CAVITY PLUS SAMPLE

In general, the sample can be analyzed as a function i = f(E,H) which represents the behavior of the charge carriers and the lattice contribution with the equivalent circuit model.

The whole system, cavity plus sample, is illustrated by Figure 11, where $C_T = C + g^2 C_o$. The system is represented by the state variables, q, the charge on C_T, and ϕ, the flux in L. Figure 11b is equivalent to Figure 11a. Then

$$\dot{q} = \frac{q}{R_T C_T} - \frac{\phi}{L} - i' + \frac{V_{in}}{R_o}$$

$$\dot{\phi} = \frac{q}{C_T}$$

where the output is $\frac{q}{C_T} = V_c$ and $R_T = \frac{R_o R}{R_o + R}$.

In matrix notation

$$\begin{bmatrix} \dot{q} \\ \dot{\phi} \end{bmatrix} = \begin{bmatrix} -\frac{1}{R_T C_T} & -\frac{1}{L} \\ \frac{1}{C_T} & 0 \end{bmatrix} x \begin{bmatrix} q \\ \phi \end{bmatrix} + \begin{bmatrix} \frac{1}{R_o} \\ 0 \end{bmatrix} V_{in} + \begin{bmatrix} -q \\ 0 \end{bmatrix} i. \qquad [23]$$

Using Eq. [16]

$$\begin{bmatrix} \dot{x} \\ \dot{v}_x \\ \dot{y} \\ \dot{v}_y \end{bmatrix} = \begin{bmatrix} 0 & 1 & 0 & 0 \\ -\omega_{p1}^2 & -\frac{1}{\tau} & 0 & -\omega_{c1} \\ 0 & 0 & 0 & 1 \\ 0 & \omega_{c2} & -\omega_{p2}^2 & -\frac{1}{\tau} \end{bmatrix} x \begin{bmatrix} x \\ v_x \\ y \\ v_y \end{bmatrix} + \begin{bmatrix} 0 \\ -\frac{e}{m^*} \\ 0 \\ 0 \end{bmatrix} E \qquad [16]$$

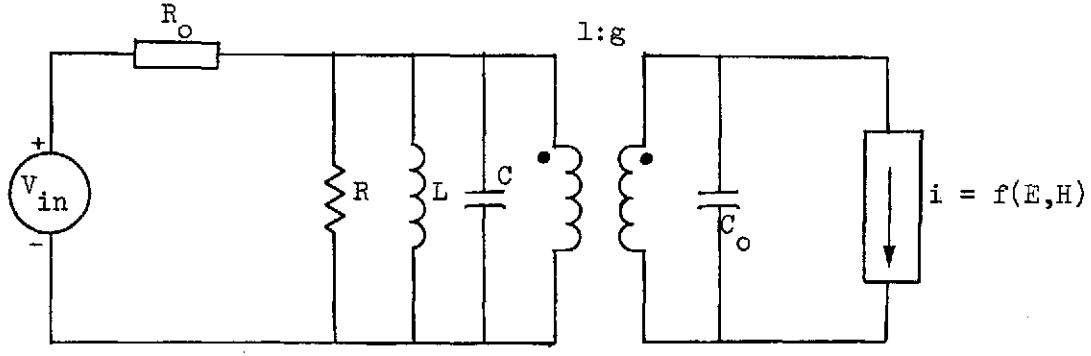

FIGURE 11a. Equivalent circuit for a general sample.

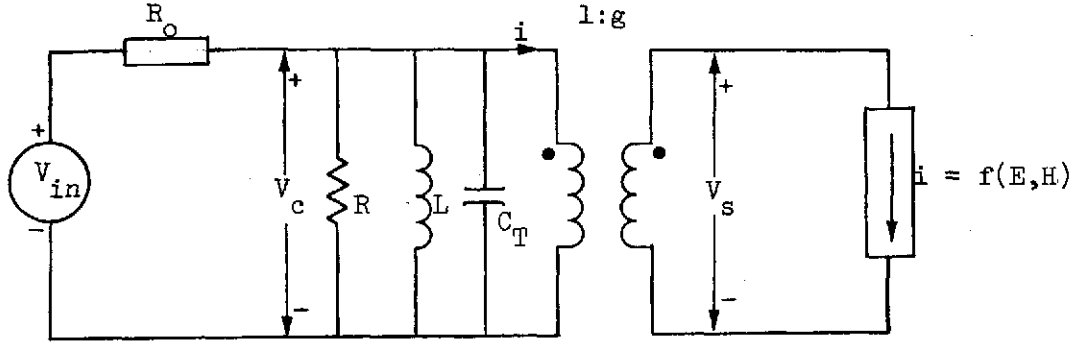

FIGURE 11b. Equivalent circuit for a general sample.

where $E = V_s/\ell_s = g\ell V_c/\ell_s = g(1/C_T\ell_s)q$, we substitute for the sample current $i = -(nev_x + \dot{n}ex)A_s$, represent the whole system by a 6th order matrix as:

$$\begin{bmatrix} \dot{q} \\ \dot{\phi} \\ \dot{x} \\ \dot{v}_x \\ \dot{y} \\ \dot{v}_y \end{bmatrix} = \begin{bmatrix} -\frac{1}{R_T C_T} & -\frac{1}{L} & \dot{n}egA_s & negA_s & 0 & 0 \\ \frac{1}{C_T} & 0 & 0 & 0 & 0 & 0 \\ 0 & 0 & 0 & 1 & 0 & 0 \\ -\frac{e}{m^*}\frac{g}{C_T\ell_s} & 0 & -\omega_{pl}^2 & -\frac{1}{\tau} & 0 & -\omega_{cl} \\ 0 & 0 & 0 & 0 & 0 & 1 \\ 0 & 0 & 0 & \omega_{c2} & -\omega_{p2}^2 & -\frac{1}{\tau} \end{bmatrix} x \begin{bmatrix} q \\ \phi \\ x \\ v_x \\ y \\ v_y \end{bmatrix} + \begin{bmatrix} \frac{1}{Ro} \\ 0 \\ 0 \\ 0 \\ 0 \\ 0 \end{bmatrix} V_{in} \qquad [24]$$

6. CALCULATION OF THE PARAMETERS OF THE MODEL

All the system parameters in Eq. [24] can be measured experimentally and predicted theoretically. They can be classified as cavity parameters (those concerning the unloaded cavity), and sample parameters, (those used to describe the sample).

The unloaded cavity parameters are R, C. L. They can be computed from the following relations:

$$L = \frac{1}{\omega_o}\left(\frac{R}{Q_o}\right)$$

$$C = \frac{1}{\omega_o}\left(\frac{R}{Q_o}\right)^{-1} \qquad [25]$$

$$R = Q_o\left(\frac{R}{Q_o}\right)$$

where ω_o and Q_o are determined directly by measurement. The value of the ratio R/Q_o is found by changing the capacitance of the cavity (without disturbing the current distribution) and measuring the corresponding change

in the resonant frequency. The change in capacitance is accomplished by varying the dielectric constant of the dielectric inside the cavity, or by a small variation of the boundary of the cavity in the region of high electric field[12]. The relation is

$$\frac{R}{Q_o} = \frac{2}{\omega_o^2} \frac{d\omega_o}{dC} . \qquad [26]$$

The theoretical developments of these parameters are found in reference 13 for a circular cylindrical resonator and in reference 14 for a re-entrant cylindrical cavity.

The g factor can be computed by measuring the resonant frequency ω_o of the cavity twice, once with a known sample present and again without it. These measurements give:

$$\omega_o^2 = \frac{1}{LC} \qquad \text{and} \qquad \omega_{o1}^2 = \frac{1}{LC_T} \qquad [27]$$

where, by definition of $C_T = C + g^2 C_o$, we obtain

$$g^2 = \frac{C_T - C}{C_o} . \qquad [28]$$

The relation between the parameter g and the filling factor η, obtained from the perturbation theory[15], is

$$\frac{\Delta\omega}{\omega_o} = \eta\left(\frac{1}{K_1} - \frac{1}{K_2}\right) = \eta \frac{K_\ell - 1}{K_\ell} \qquad [29]$$

for $K_1 = 1$ and $K_2 = K_\ell$ where K_1 and K_ℓ are the dielectric constants of free space and the sample, respectively. Combining [27], [28] and [29] we find the relation

$$\eta = g^2 \frac{C_o}{2C_T} = \frac{\Delta\omega}{\omega_o} \qquad [30]$$

7. ANALOG SIMULATION

Our approach to study all the cases mentioned before is to write the equations which represent the system in a state form, and use the standard method to find the solution. In the simpler case we will deal with 4 x 4 matrix, and the computation of the poles (natural frequencies of the system) is not a problem if we have the computer facilities. However, we don't have a general expression for the solution of the system in terms of its parameters. We can only have solutions for discrete values of the parameters. The system becomes complicated if some of the parameters are varying with time. The LaPlace transform method is not useful, and the solution for a time varying case can be quite involved.

In these cases, a simulation of the system with the analog computer[16] will help us to find its response. We simulate the case of the cavity and sample with free electrons only when a constant magnetic field and a microwave electric field was applied. The state equation is represented by Eq. [24]. For this case, we have a 6 x 6 matrix. This is the union of 2 x 2 matrix corresponding to the cavity and a 4 x 4 matrix corresponding to the sample, plus some interaction terms which couple the two systems. The first system has a high Q ($\simeq 10^4$) and the second low Q ($\simeq 1$). We study the behavior of the low Q system through one of the state variables of the high Q system (voltage of the cavity).

When an input voltage V_{in} is applied to the system, the state variable $V_c = q_T/C_T$ will be the sum of six terms with different frequencies and amplitudes. We assume that 4 of the terms, those corresponding to the low Q system are small and are neglected. The other two, corresponding to the high Q system will stay longer, and they will give information on the

whole system, including the sample through the coupling of interacting terms. The information is in the frequency and in the amplitude of the response of the two state variables. (Voltage and current of the cavity).

Then we can assume that we have a second order system as long as the coupling and the Q of the sample are small. It is only in this case that we characterize the system in terms of a single resonant frequency of the cavity and a single Q. If we assume this type of solution, then we will observe in all the cases that the two state variables corresponding to the cavity are purely sinusoidals. We can then measure its frequency and its damping rate for different values of the sample parameters.

Figure 12 shows the circuitry assembled to simulate the Eq. [24]. The circuit is divided in three parts corresponding to the cavity, plasma and magnetic properties. Each part has two integrators for two state variables which are the voltage and current for the cavity, the position and velocity in the x direction for the plasma properties, and the position and velocity in the y direction for the magnetic properties.

The values required to simulate an experiment are: the resonant frequency of the cavity ω_o, the cavity Q, the filling factor of sample η, the relaxation time for the free electrons in the sample, and different values of plasma and cyclotron resonant frequencies. The following values were chosen:

$$\omega_o = 2\pi 9 \times 10^9 \text{ Hz}$$

$$Q = 10^4$$

$$10^{-13}_{\text{sec}} < \tau < 10^{-10}_{\text{sec}}$$

$$\eta = 1.25 \times 10^{-3}$$

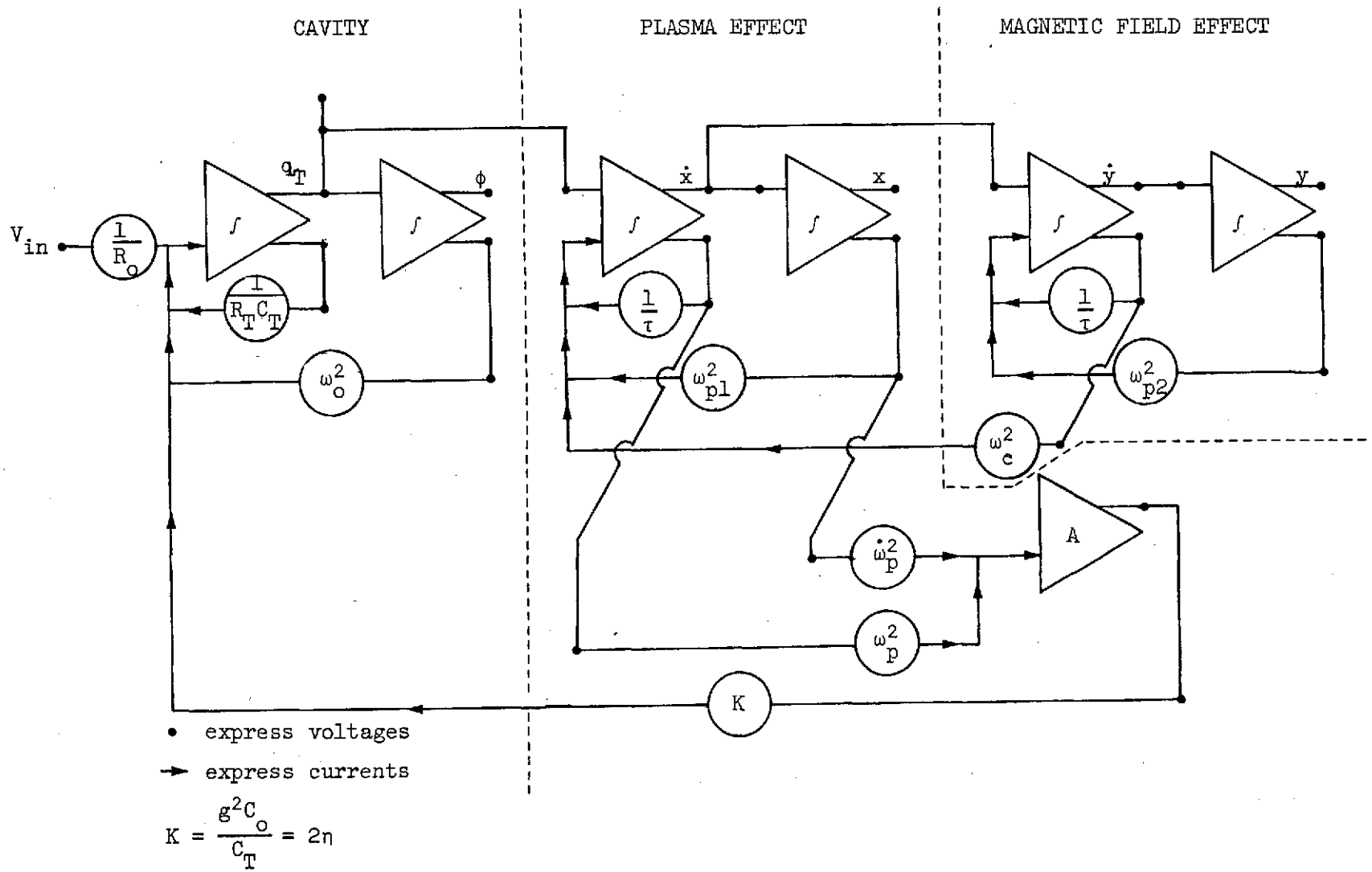

FIGURE 12. Analog equivalent circuit to simulate the PDE in a static magnetic field.

ω_o was chosen as the normalized frequency. To study the frequency response of the circuit, a voltage impulse is applied and the trajectories of the state variables are recorded. Figure 13 shows the expected trajectory for the two state variables.

After observing a sinusoidal response, the analog circuit is calibrated in the following way:

FIRST: Only the cavity section is connected. The state variables are recorded on the two channels (xy) of a recorder or plotter. The trajectory starts at position 0 at time t = 0, which is the initial condition. The trajectory goes to position 1 at time t_1. The trajectory is similar to Figure 13, and the initial and final position are shown in Figure 14 for different values of Q. In this case, t_1 = 94 sec, and the trajectory is made by 148 complete revolution plus the fraction shown. When the cavity Q is large the locus terminal point is outside the corresponding point when the Q is small. The radial scale is related to Q, and the angle change represents frequency change.

SECOND: The part of the circuit representing the plasma properties of the sample is included in the second experiment. The Q of the cavity was set at 10^4 and the filling factor $\eta = 1.25 \times 10^{-3}$. The experiment is performed for different values of ω_p^2 and the results are shown in Figure 15. We observe how the frequency and Q change for different values of ω_p. The relation between the change in angle degrees shown in Figure 16 and the change in resonant frequency of the cavity is expressed by $a = \Delta f_o/\Delta\theta$, which is specified in each figure. Different figures are shown for different values of τ.

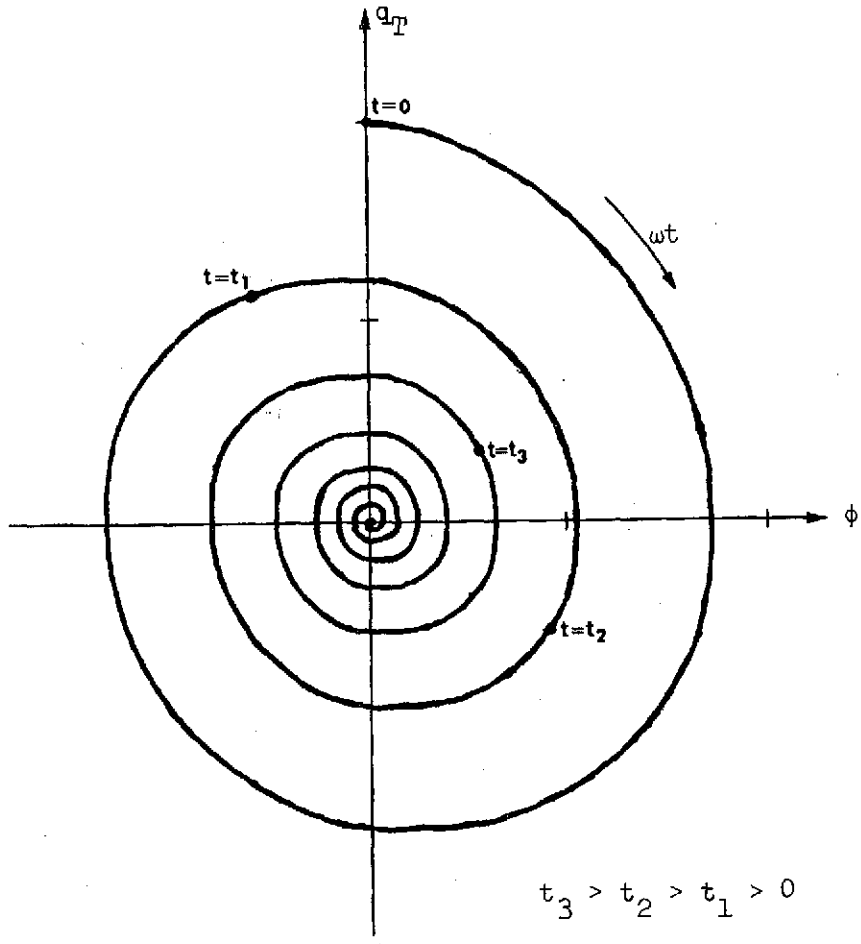

FIGURE 13. Expected qualitative trajectory for the two state variables corresponding to the cavity.

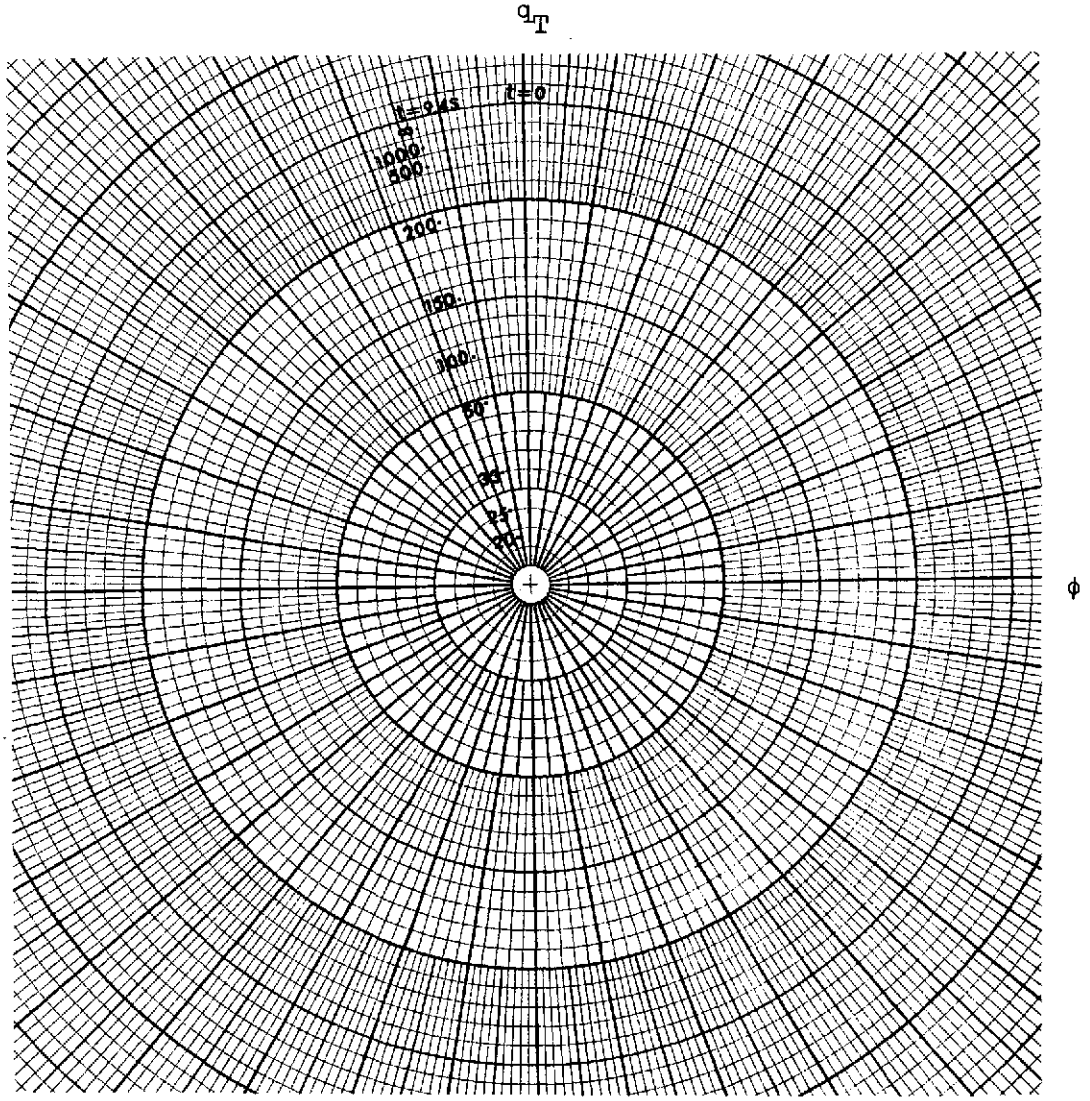

FIGURE 14. Analog simulation of the microwave cavity. Different values of cavity Q cause different positions at t = 94 sec.

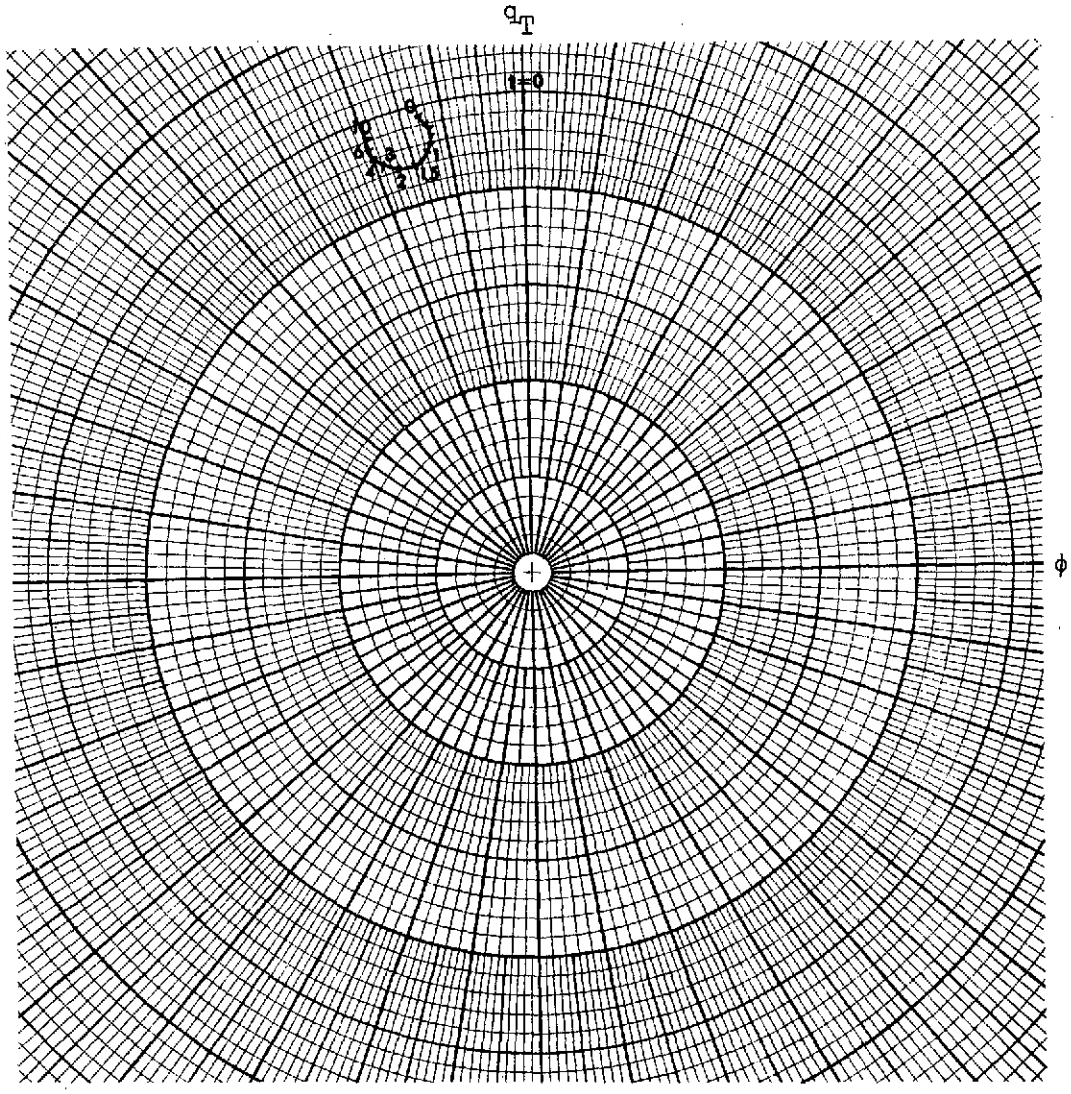

FIGURE 15a. Analog simulation of the cavity with the sample for different values of ω_p^2/ω_o^2

$\tau = 1.2 \times 10^{-11}$ sec.

$K = 0.0025$

$\omega_c^2 = 0.000$

$a = \frac{\Delta f}{\Delta \theta} = .106$ MHz/angle degree

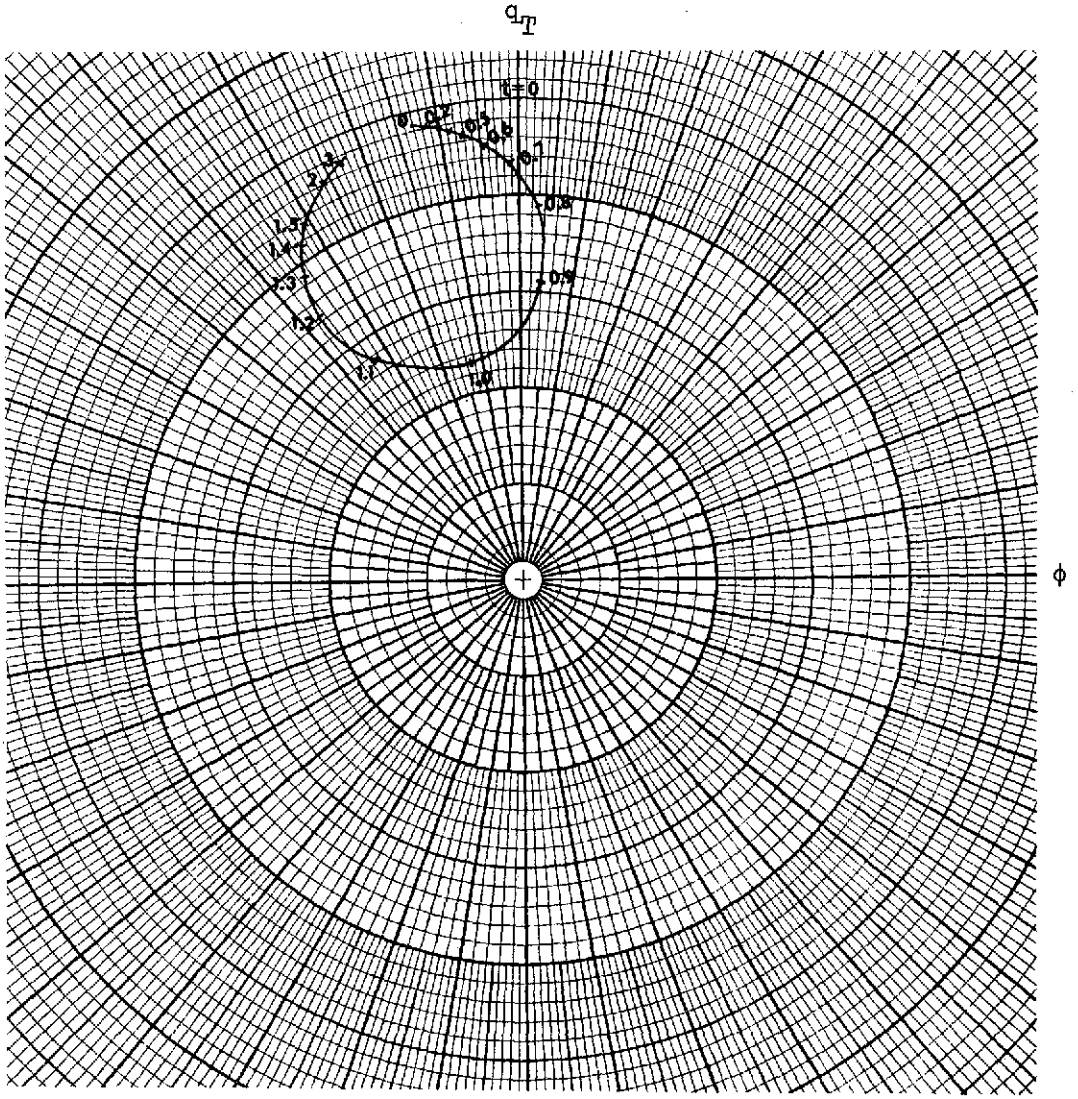

FIGURE 15b. Analog simulation of the cavity with the sample for different values of ω_p^2/ω_o^2

$\tau = 1.2 \times 10^{-10}$ sec.

$K = 0.0025$

$\omega_c^2 = 0.000$

$a = \frac{\Delta f}{\Delta \theta} = .106$ MHz/angle degree

THIRD: The part of the circuit corresponding to magnetic properties is connected. Figure 16 shows the results for different ω_c, ω_{p1} and ω_{p2}. The differences between ω_{p1} and ω_{p2} are due to different values of depolarization factor L for x and y directions.

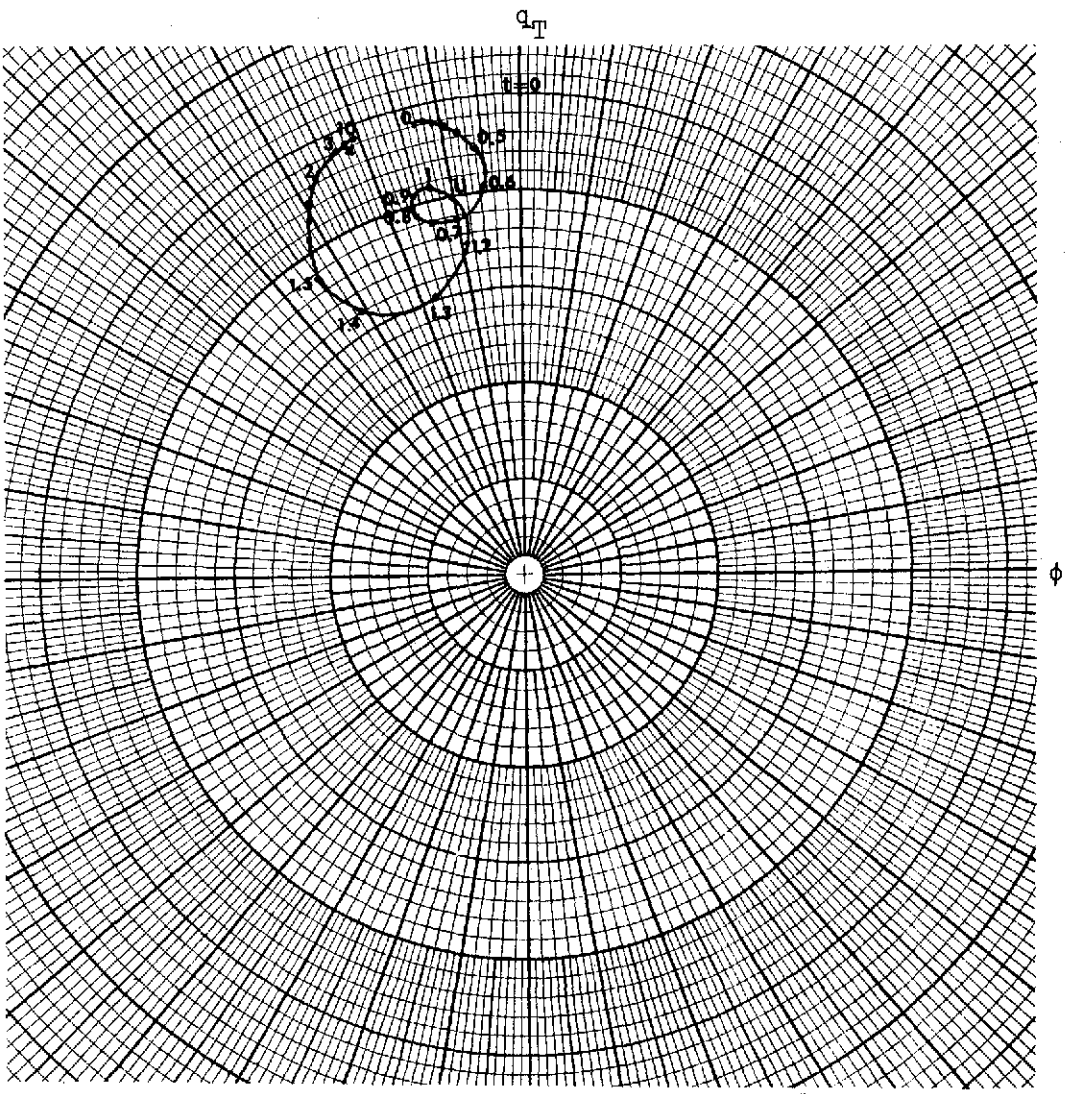

FIGURE 16a. Analog simulation of the cavity with the sample for different values of ω_p^2/ω_o^2, a static magnetic field and:

$\tau = 1.2 \times 10^{-10}$ sec.

$K = 0.0025$

$\omega_c^2 = 0.1\ \omega_o^2$

a = .106 MHz/angle degree

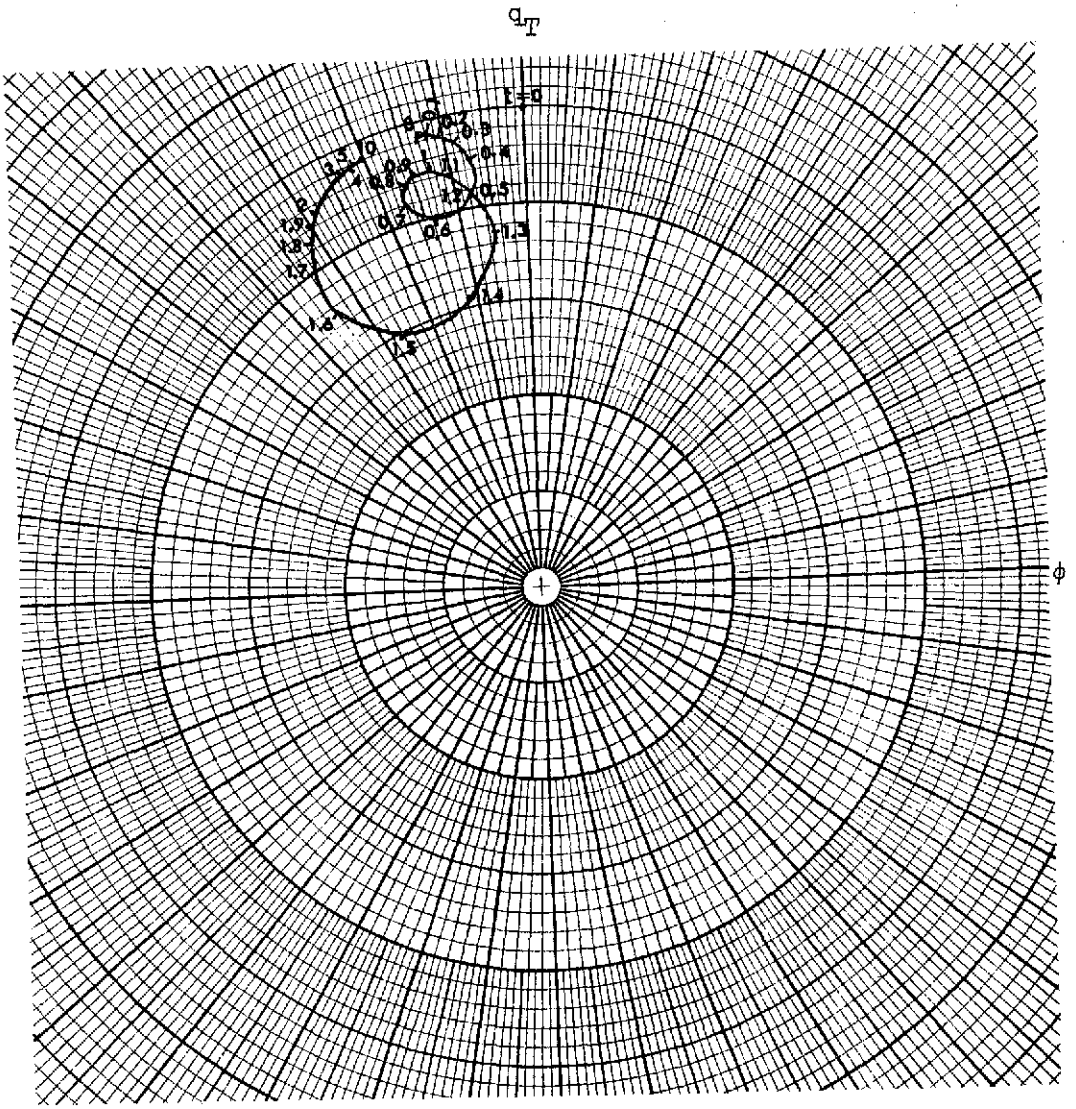

FIGURE 16b. Analog simulation of the cavity with the sample for different values of ω_p^2/ω_o^2, a static magnetic field and:

$\tau = 1.2 \times 10^{-10}$ sec.

$K = 0.0025$

$\omega_c^2 = 0.2\ \omega_o^2$

a = .106 MHz/angle degree

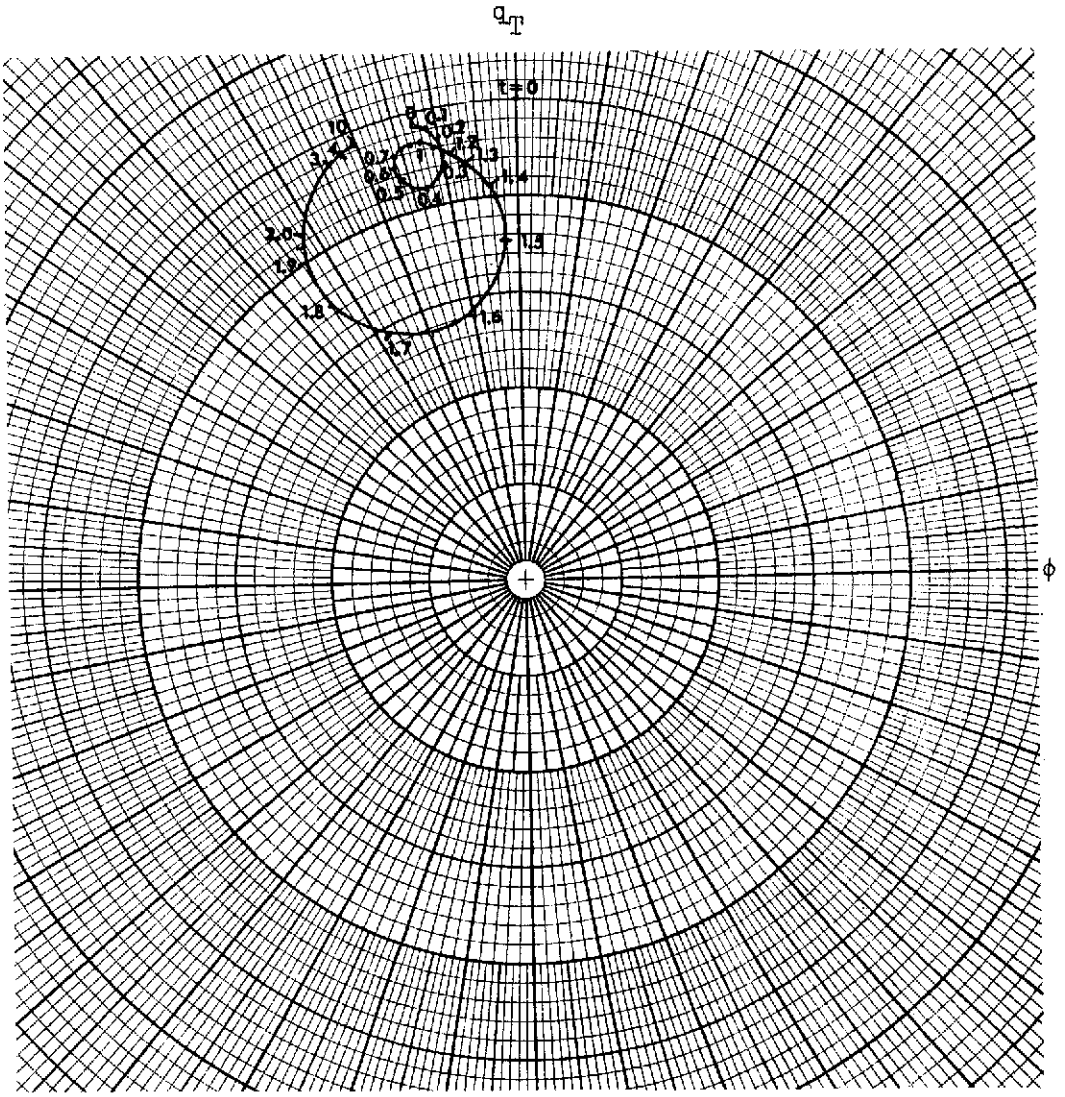

FIGURE 16c. Analog simulation of the cavity with the sample for different values of ω_p^2/ω_o^2, a static magnetic field and:

$\tau = 1.2 \times 10^{-10}$ sec.

$K = 0.0025$

$\omega_c^2 = 0.4\ \omega_o^2$

$a = .106$ MHz/angle degree

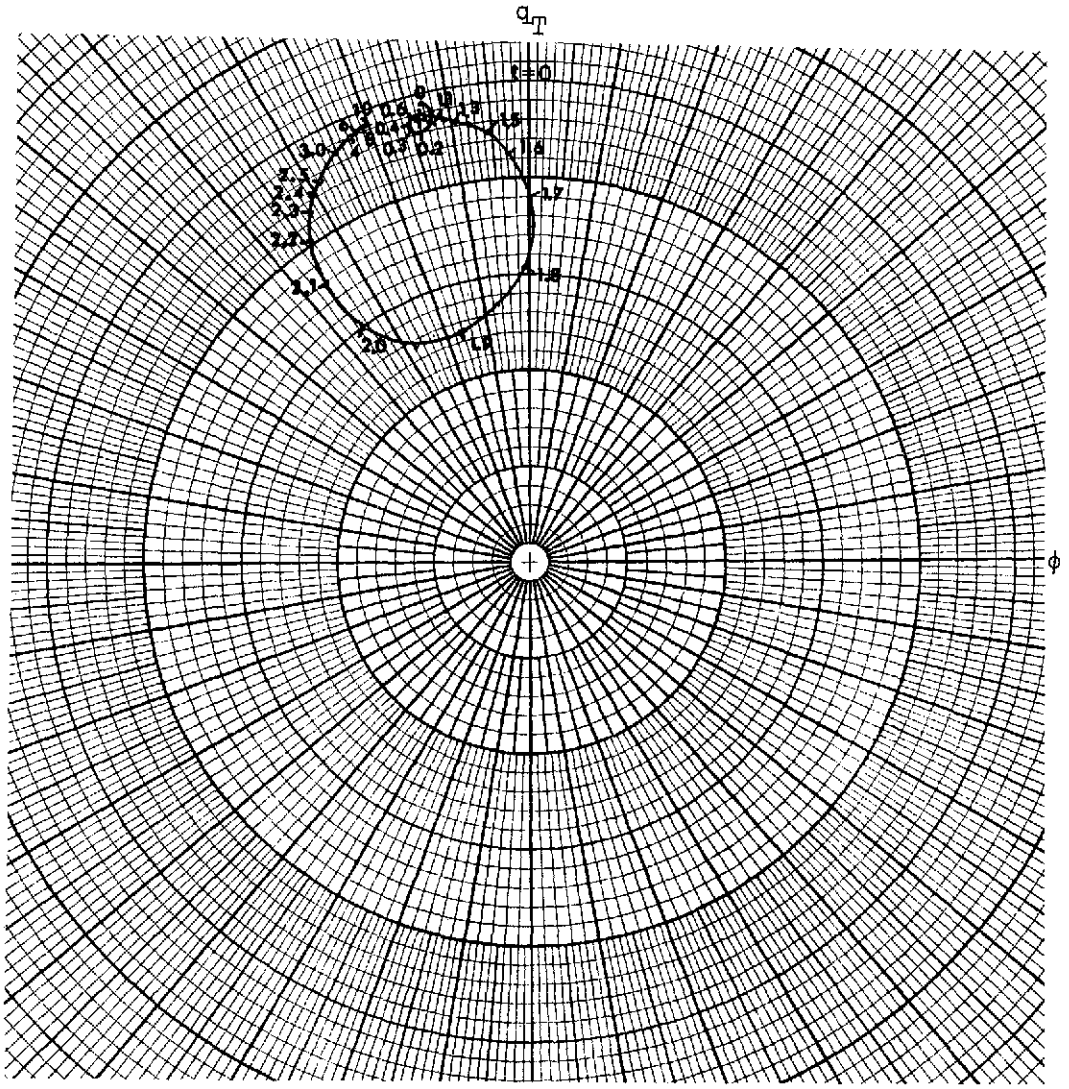

FIGURE 16d. Analog simulation of the cavity with the sample for different values of ω_p^2/ω_o^2, a static magnetic field and:

$\tau = 1.2 \times 10^{-10}$ sec.

$K = 0.0025$

$\omega_c^2 = 0.8\ \omega_o^2$

a = .106 MHz/angle degree

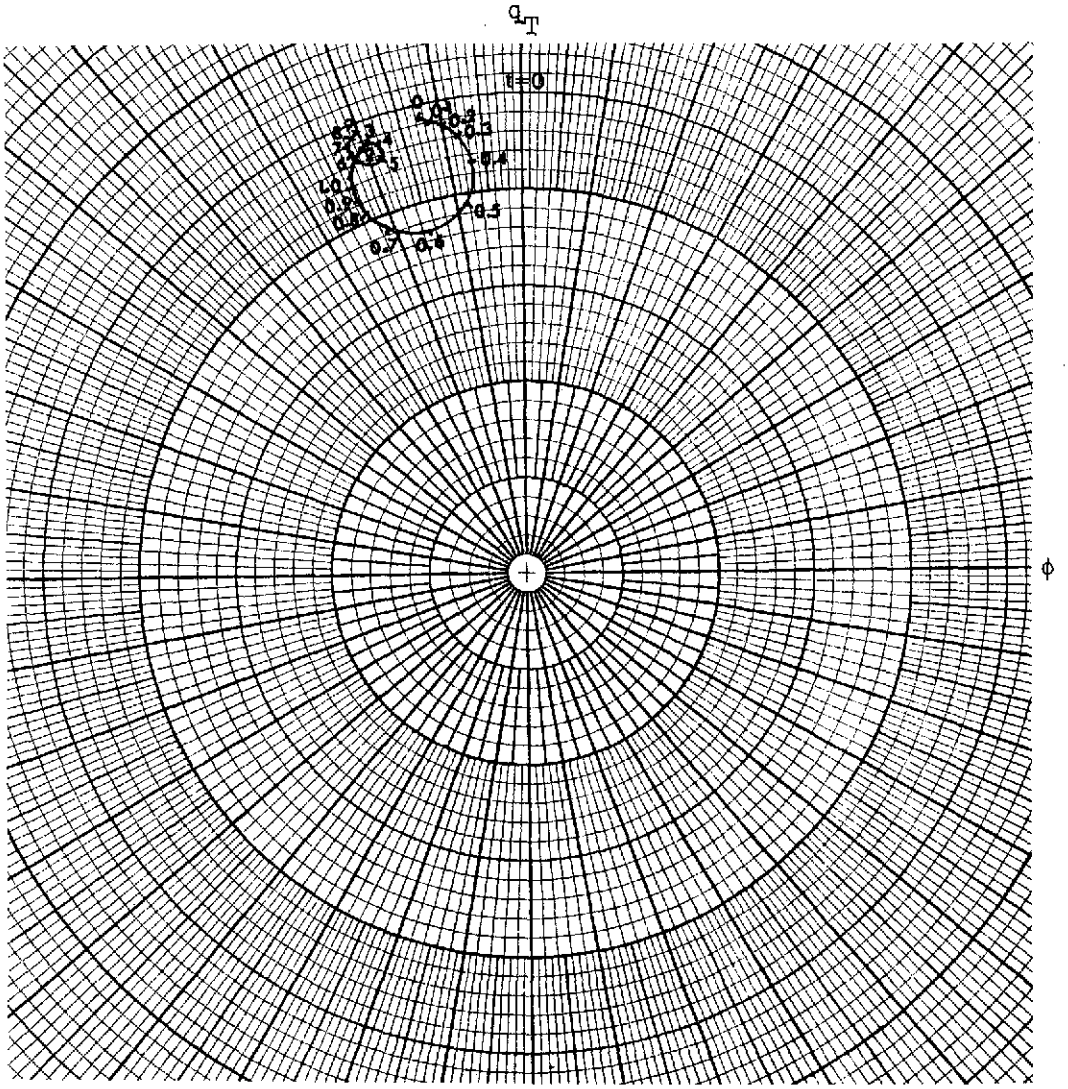

FIGURE 16e. Analog simulation of the cavity with the sample for different values of ω_p^2/ω_o^2, static magnetic field and:

$\tau = 1.2 \times 10^{-10}$ sec.

$K = 0.0025$

$\omega_e^2 = 0.4\ \omega_o^2$

$a = 0.106$ MHz/angle degree

$\omega_{p1}^2 = \omega_{p2}^2 = 0.2\omega_p^2$

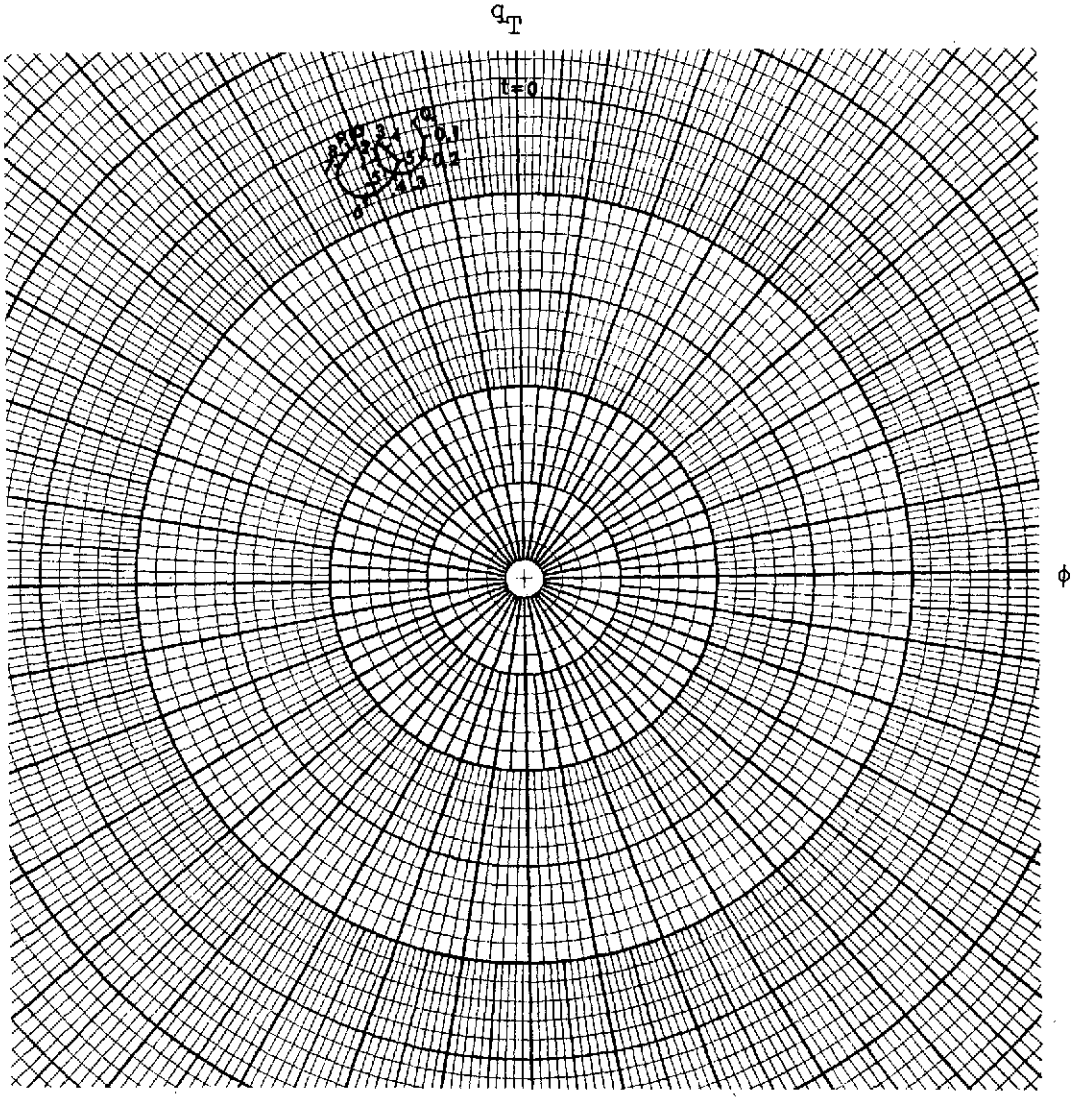

FIGURE 16f. Analog simulation of the cavity with the sample for different values of ω_p^2/ω_o^2, static magnetic field and:

$\tau = 1.2 \times 10^{-10}$ sec.

$K = 0.0025$

$\omega_c^2 = 0.8\ \omega_o^2$

$a = 0.106$ MHz/angle degree

$\omega_{p1}^2 = \omega_{p2}^2 = 0.2\omega_p^2$

CHAPTER II.

ANALYSIS OF THE CIRCUIT FOR THE P.D.E. SYSTEM

1. INTRODUCTION

The mechanisms which produce the changes in resonant frequency of the microwave cavity are discussed in Chapter I. This chapter is devoted to analyzing the methodology used to measure the change in cavity resonant frequency continuously. The circuit used to accomplish this is similar to the one designed by R.V. Pound[17] for frequency stabilization of microwave oscillators with a high Q resonant cavity. Figure 17 is a block diagram of Pound's system.

In this system, the discriminator circuit develops a voltage which is a measure of the difference between the oscillator frequency and the cavity resonant frequency. When this voltage is amplified and superimposed in the correct sense on the supply voltage of an element of the oscillator (i.e., the reflector voltage for a klystron) the frequency error is reduced. In this way the oscillator follows the cavity resonant frequency.

It is important to note that Pound's circuit oscillator adjusts itself to the constant resonant frequency of the cavity. In the present case, however, the resonant frequency is not constant, but it varies according to the electro-optic properties of the semiconductor crystal sample inside the cavity.

The following analysis is limited to the study of variations in the oscillator frequency caused by the sample inside the cavity. The sample and cavity are considered first, then the system as a whole, and Chapter III presents a summary of conclusions.

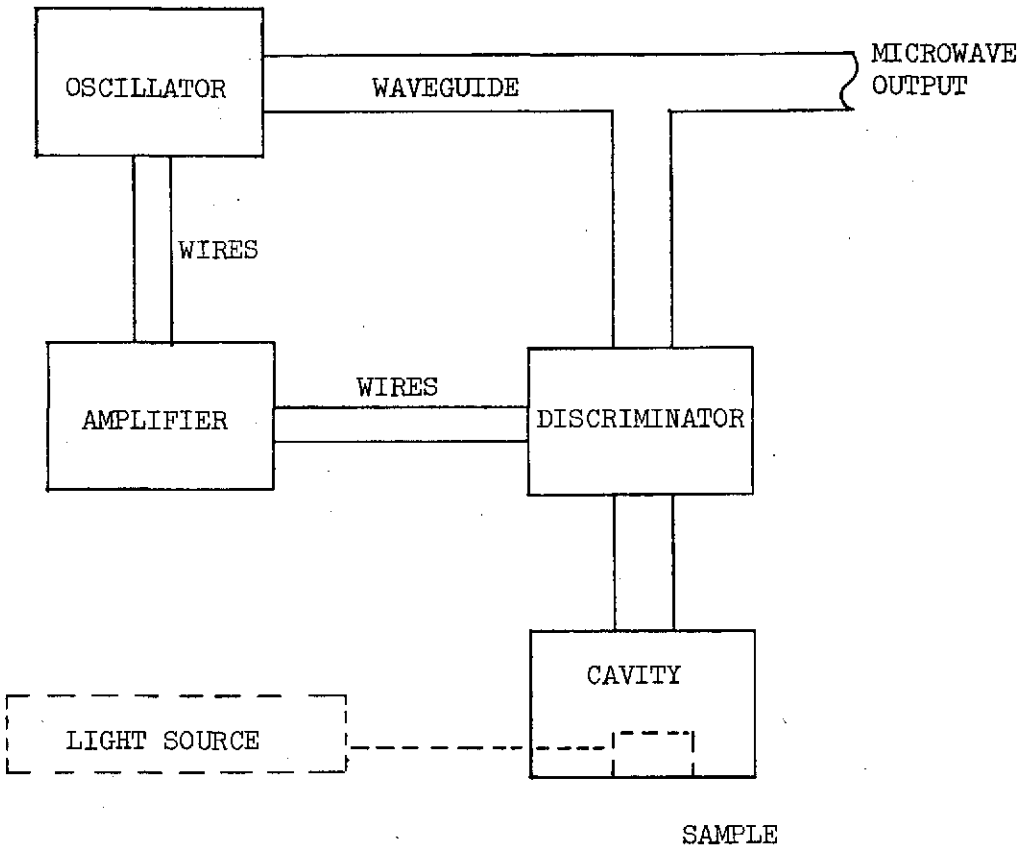

FIGURE 17. Block diagram of the detector system.

2. SAMPLE ANALYSIS

Figure 3 in Chapter I represents the sample equivalent circuit in its simplest form. The admittance of the circuit shown in Figure 3 is

$$Y(\omega) = j\omega C_o + \frac{1}{j\omega L_s + R_s + \frac{1}{j\omega C_o}}$$

or

$$Y(\omega) = G(\omega) + jB(\omega) \qquad [31]$$

The real and imaginary components are

$$G(\omega) = \left[\frac{\frac{\omega_p^2}{\omega^2} \cdot \frac{1}{\omega\tau}}{(\frac{\omega_p^2}{\omega^2} - 1)^2 + \frac{1}{\omega^2\tau^2}}\right]\omega C_o = G(\frac{\omega_p^2}{\omega^2}, \omega\tau) \qquad [32]$$

and

$$B(\omega) = \left[\frac{\frac{\omega_p^2}{\omega^2}(\frac{\omega_p^2}{\omega^2} - 1)}{(\frac{\omega_p^2}{\omega^2} - 1)^2 + \frac{1}{\omega^2\tau^2}}\right]\omega C_o + \omega C_o = B(\frac{\omega_p^2}{\omega^2}, \omega\tau) \qquad [33]$$

where

$$\omega_p^2 = \frac{1}{LC_o} = \frac{ne^2}{m^*\varepsilon_\ell},$$

$$R_s = \frac{m^*\ell}{ne^2A\tau},$$

$$L_s = R_s\tau,$$

$$C_o = \frac{\varepsilon_\ell A}{\ell}.$$

The derivatives of $G(\frac{\omega_p^2}{\omega^2}, \omega\tau)$ and $B(\frac{\omega_p^2}{\omega^2}, \omega\tau)$ with respect to ω_p^2 are:

$$G'(\frac{\omega_p^2}{\omega^2}, \omega\tau) = \left[\frac{1 - \frac{\omega_p^4}{\omega^4} + \frac{1}{\omega^2\tau^2}}{[(1 - \frac{\omega_p^2}{\omega^2})^2 + \frac{1}{\omega^2\tau^2}]^2}\right] \cdot \frac{C_o}{\omega^2\tau} \qquad [34]$$

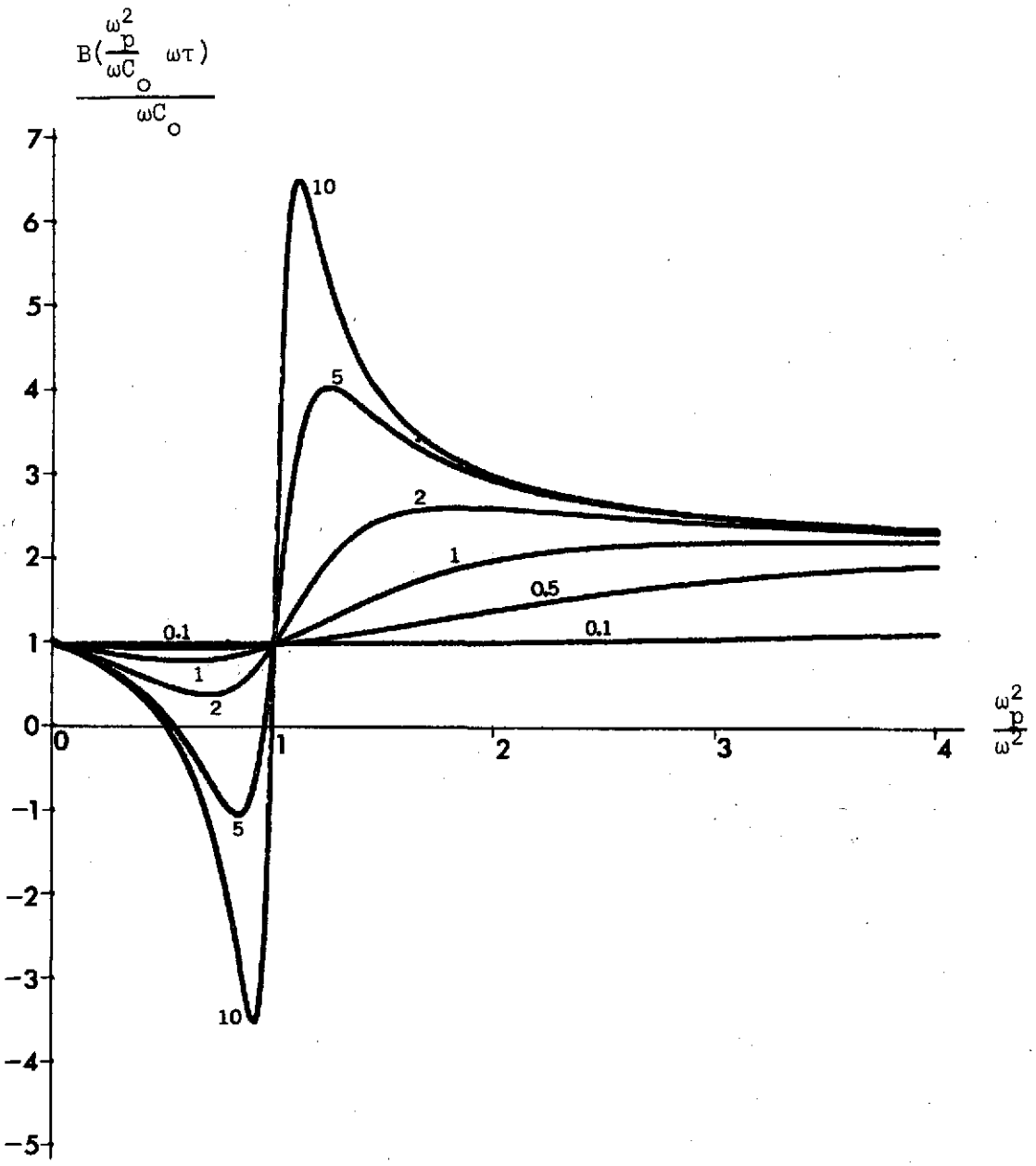

FIGURE 18. Susceptance of the sample for different values of $\omega\tau$ product and ω_p^2/ω^2.

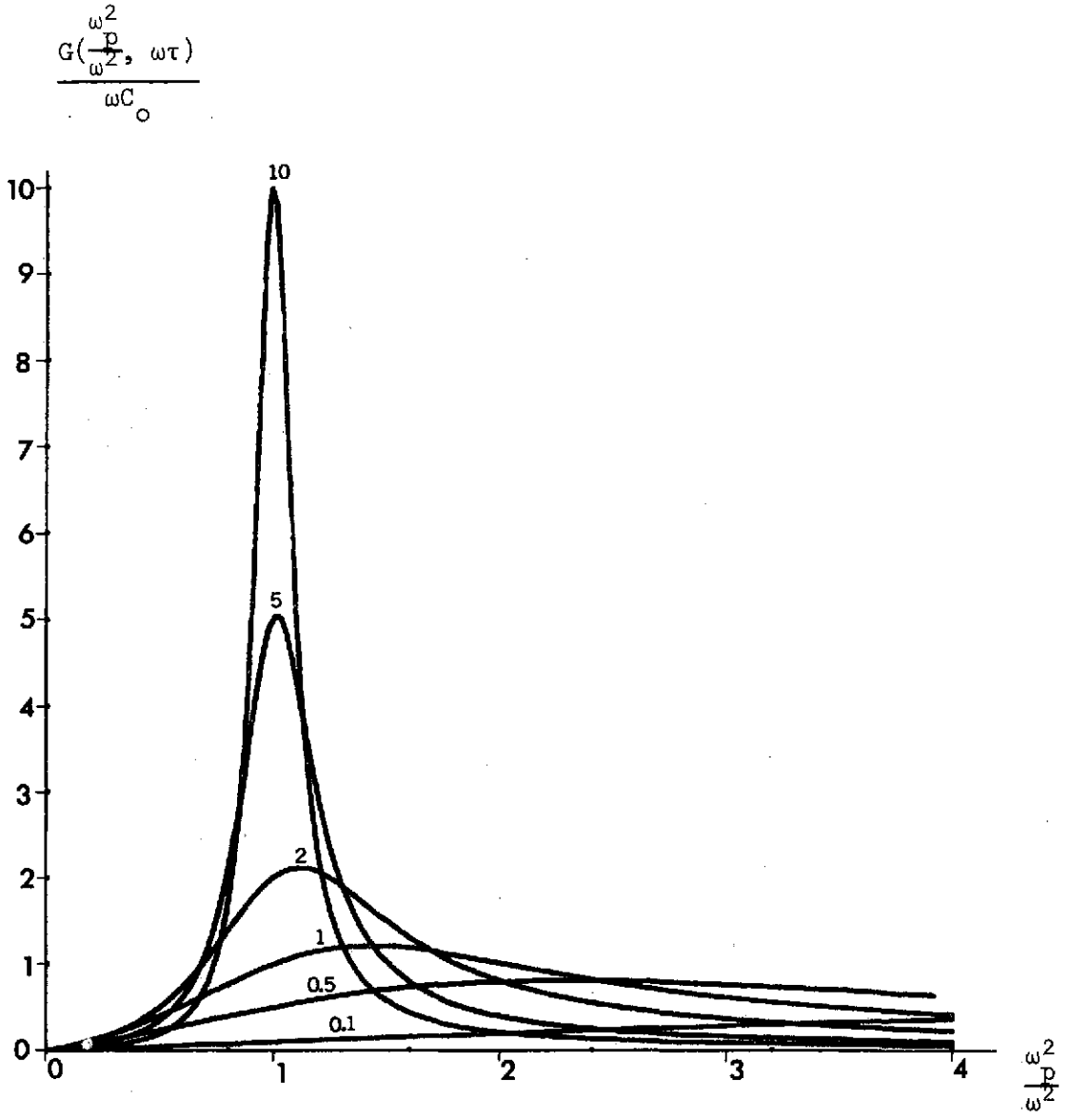

FIGURE 19. Conductivity of the sample for different values of $\omega\tau$ product and ω_p^2/ω^2.

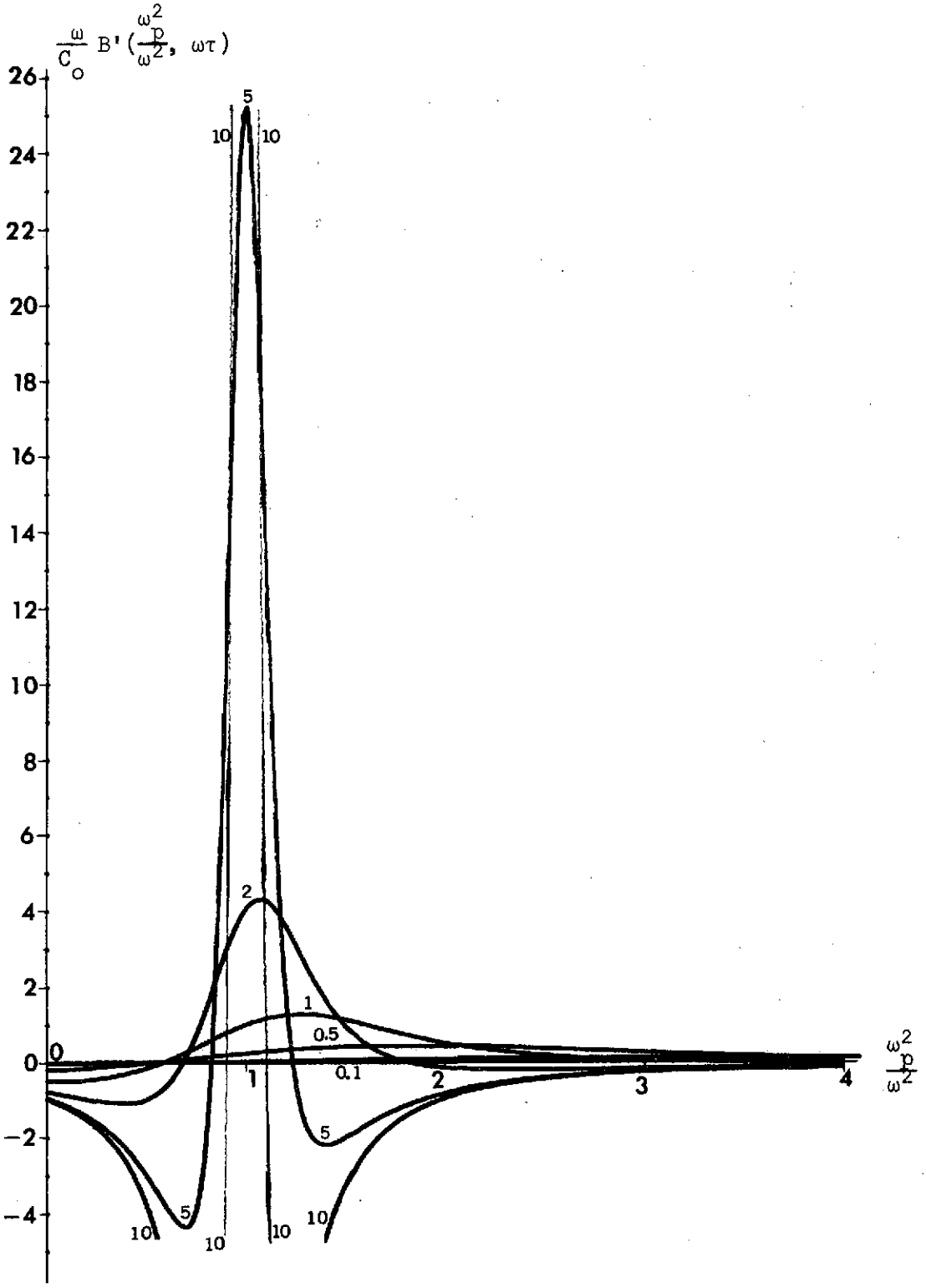

FIGURE 20. Slope of the susceptance for different values of $\omega\tau$ product and ω_p^2/ω^2.

$$B'\left(\frac{\omega_p^2}{\omega^2}, \omega\tau\right) = \left[\frac{-1}{\left(\frac{\omega_p^2}{\omega^2} - 1\right)^2 + \frac{1}{\omega^2\tau^2}} + \frac{\frac{2\omega_p^2}{\omega^4\tau^2}}{\left[\left(\frac{\omega_p^2}{\omega^2} - 1\right)^2 + \frac{1}{\omega^2\tau^2}\right]^2}\right] \frac{C_o}{\omega}. \qquad [35]$$

Eqs. [32], [33], and [35] are shown in Figures 18, 19 and 20, respectively for various $\omega\tau$ products. Observing this figure, we can choose the following three regions:

Region I	$\omega_p < \omega$
Region II	$\omega_p \simeq \omega$
Region III	$\omega_p > \omega$.

In each of the three regions, there is a maximum value for $|B'|$.

3. CHANGE OF THE CAVITY RESONANT FREQUENCY DUE TO A CHANGE IN THE SUSCEPTIBILITY OF THE SAMPLE

The model for the cavity plus the sample is represented by the circuit of Figure 9 in Chapter I. The resonant frequency of the circuit of Figure 9 is ω_o such that

$$\omega_o C_T - \frac{1}{\omega_o L} + g^2 B\left(\frac{\omega_p^2}{\omega_o^2}, \omega_o\tau\right) = 0$$

where $C_T = C + g^2 C_o$, and solving for ω_o

$$\omega_o \simeq \omega_c - \frac{g}{2C_T} B\left(\frac{\omega_p^2}{\omega_o^2}, \omega_o\tau\right)$$

from which can be computed the change in the cavity resonant frequency, given by Eq. [36]

$$\Delta f_o = \frac{\Delta\omega_o}{2\pi} = -\frac{g^2}{2\pi C_T} \Delta B\left(\frac{\omega_p^2}{\omega_o^2}, \omega_o\tau\right). \qquad [36]$$

4. THE MICROWAVE DISCRIMINATOR[17]

A microwave phase discriminator is constructed with the cavity, two magic tees and two detector diodes. It is illustrated by Figure 21.

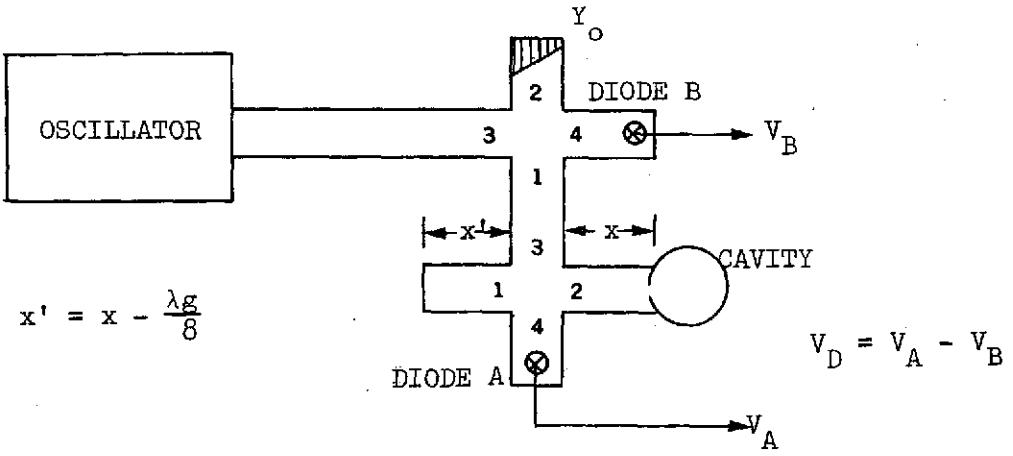

FIGURE 21a. The microwave frequency discriminator.

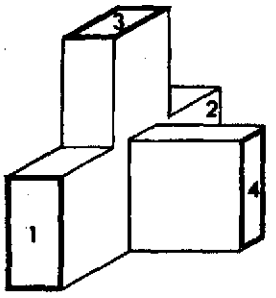

FIGURE 21b. Magic T

The output voltage of the discriminator is

$$V_D = PD \frac{\alpha a}{(1 + \alpha)^2 + a^2} \qquad [37]$$

where P = the power available from the matched generator connected to the discriminator,

$a = \frac{2(f - f_o)}{f_o} Q_o$,

D = the rectification efficiency of the crystals in volts per unit incident power, and

α = the ratio $\frac{Q_o}{Q_{EXT}}$.

And for a cavity representation, as in Figure 22,

$$\alpha = \frac{Q_o}{Q_{EXT}} = \frac{m^2 R}{R_o}$$

where $Q_o = \omega_o RC$

$Q_{EXT} = \frac{\omega_o CR_o}{m^2}$.

The rate of change of the discriminator voltage with frequency is greatest at resonance, or $a \simeq 0$, and it is

$$\frac{dV_D}{df} = DP \frac{Q_o}{f_o} \cdot \frac{2\alpha}{(1 + \alpha)^2}. \qquad [38]$$

This expression has its maximum value for α equal to 1, and for the frequency stabilization circuit this is the optimum value of α. ($\alpha = 1$ implies $Q_o = Q_{EXT}$ or $m^2 = R_o/R$ which is the critical coupling condition). The value of dV_D/df for $\alpha = 1$ is

$$\frac{dV_D}{df} = \frac{DP}{2} \frac{Q_o}{f_o} = \frac{DP}{4B_W} \qquad [39]$$

where $B_W = \frac{1}{2}\Delta f_{cavity}$.

The voltage output of the discriminator can be written approximately as

$$V_D = \frac{DP}{4B_W} \Delta f \qquad [40]$$

for $\Delta f = f - f_o < B_W$ = cavity bandwidth.

The main sources of noise in the discriminator are the diode noise, and the differences in the characteristics of the two diodes. These produce an output voltage V_{nD}, and the final discriminator voltage V_D' will be

$$V_D' = \frac{DP}{4B_W} \Delta f + V_{nD} \qquad [41]$$

Up to this point, we have considered the case where the cavity Q is a constant Q_o and does not depend on the density of free carriers in the sample. This is true if the losses associated with the sample are smaller than the cavity losses. However, when the filling factor η is increased in order to get a higher response, the cavity Q depends mainly on the losses associated with the power absorbed by the free carriers in the sample. Considering this, a change in the density of free carriers induces a variation in the cavity resonant frequency f_o and also in the cavity Q. Then, from Eq. [37] we consider three cases depending on the relative values of α in which, for each case, there will be two different values of free carrier density denoted by sub-indices 1 and 2.

Case a) for $\alpha_1, \alpha_2 >> 1$, or $Q_{o1}, Q_{o2} >> Q_{EXT}$, which is the overcoupled condition

$$\Delta V_D \simeq 2PDQ_E(\delta_1 - \delta_2) \simeq 2PDQ_E \frac{\Delta f_o}{f_o} \qquad [42]$$

Case b) for $\alpha_1 \simeq \alpha_2 \simeq 1$, or $Q_{o1} \simeq Q_{o2} \simeq Q_{EXT}$,

$$\Delta V_D \simeq \frac{PD}{2}(Q_{o1}\delta_1 - Q_{o2}\delta_2) \qquad [43]$$

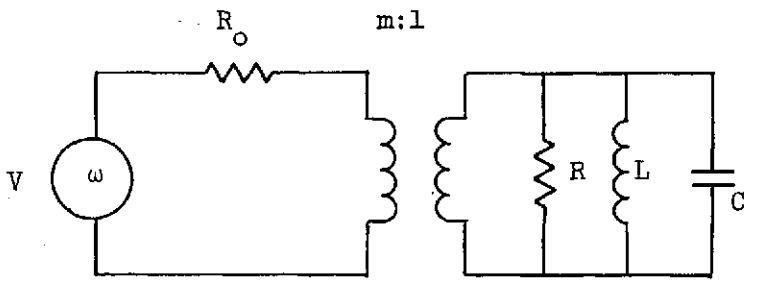

FIGURE 22. Equivalent circuit for the cavity coupled to a waveguide.

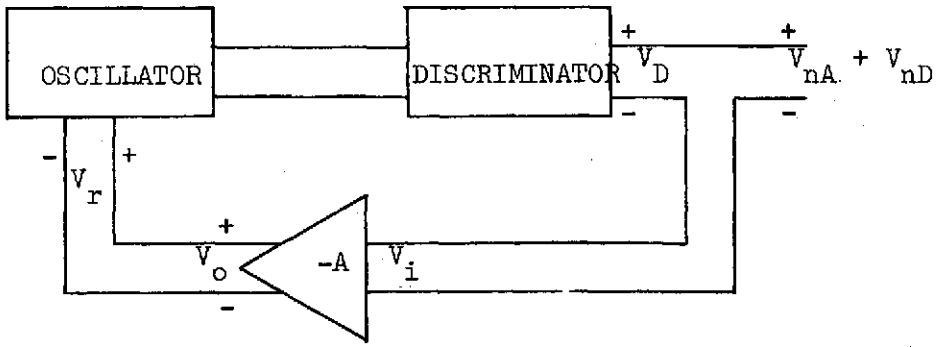

FIGURE 23. Block diagram of the feedback loop and the sources of noise.

Case c) for α_1, $\alpha_2 \ll 1$, or Q_{o1}, $Q_{o2} \ll Q_{EXT}$, which is the undercoupling condition

$$\Delta V_D \simeq 2PDQ_E(\alpha_1^2\delta_1 - \alpha_2^2\delta_2) \qquad [44]$$

where $\delta_1 = \dfrac{f - f_{o1}}{f_{o1}}$, $\delta_2 = \dfrac{f - f_{o2}}{f_{o2}}$

and $\delta_1 - \delta_2 \simeq \dfrac{f_{o2} - f_{o1}}{f_{o1}} = \dfrac{-\Delta f_o}{f_o}$

5. SELECTION OF THE OPERATION REGION

Replacing the value $\omega_o R_T C_T$ for the cavity Q, where R_T is computed from

$$\frac{1}{R_T} = \frac{1}{R_C} + \frac{g^2}{R_{sample}} = \frac{1}{R_C} + g^2 G\left(\frac{\omega_p^2}{\omega_o^2}, \omega_o\tau\right) \qquad [45]$$

we see that when the sample loads the cavity, its Q is mainly determined by the sample losses.

$$R_T = \frac{1}{g^2 G\left(\dfrac{\omega_p^2}{\omega_o^2}, \omega_o\tau\right)} . \qquad [46]$$

Then the cavity Q is

$$Q = \omega_o R_T C_T = \frac{\omega_o C_T}{g^2 G\left(\dfrac{\omega_p^2}{\omega_o}, \omega_o\tau\right)} . \qquad [47]$$

The change of the cavity resonant frequency was expressed by Eq. [36]

$$\Delta f_o = -\frac{g^2}{2\pi C_T} \Delta B\left(\frac{\omega_p^2}{\omega_o^2}, \omega_o\tau\right). \qquad [36]$$

Using Eqs. [47] and [36] in Eqs. [42], [43] and [44], we obtain the output voltage of the microwave discriminator as a function of ω_o and ω_p^2.

Case a) for α_1, $\alpha_2 \gg 1$

$$\Delta V_D = 2PDQ_E \frac{\Delta f_o}{f_o} = -\frac{2PDQ_E g^2}{2\pi C_T} \Delta B\left(\frac{\omega_p^2}{\omega_o^2}, \omega_o\tau\right) \qquad [48]$$

Taking $\Delta B(\frac{\omega_p^2}{\omega_o^2}, \omega_o\tau) = -\omega_o C_o \tau^2 \Delta\omega_p^2$ which is the maximum variation and corresponds to the Region II where $\omega_o \approx \omega_p$, and Eq. [30]

$$\eta = \frac{g^2 C_o}{2C_T} \qquad [30]$$

we have

$$\Delta V_D = \frac{PD}{4} (Q_E 16\eta\tau^2\omega_p^2) \frac{\Delta n}{n},$$

or

$$V_D = \frac{PD}{4}(\frac{Q_E}{Q_o} 8\omega_o\tau) \frac{\Delta n}{n} \qquad [49]$$

where Q_o in Region II ($\omega_o \approx \omega_p$) is

$$Q_o = \omega_o R_T C_T = \frac{\omega_o R_s C_T}{g^2} = \frac{\omega_o C_T}{g^2 C_o} C_o R_s$$

$$Q_o = \frac{\omega_o \varepsilon_\ell}{2\eta\sigma_o} = \frac{\omega_o}{2\eta\omega_p^2\tau} \qquad [50]$$

Case b) for $\alpha_1, \alpha_2 \approx 1$. Starting with Eq. [43]

$$\Delta V_D \approx \frac{PD}{2}(Q_{o1}\delta_1 - Q_{o2}\delta_2) \qquad [43]$$

where

$$Q_{oi}\delta_i = \frac{Q_o \Delta f_o}{f_o} = \frac{B_i(\frac{\omega_{pi}^2}{\omega_o^2}, \omega_o\tau)}{G_i(\frac{\omega_{pi}^2}{\omega_o^2}, \omega_o\tau)} = (\frac{\omega_{pi}^2}{\omega_o^2} - 1)\omega_o\tau, \qquad [51]$$

we obtain

$$\Delta V_D = \frac{PD}{2} \Delta \frac{B(\frac{\omega_p^2}{\omega_o^2}, \omega_o\tau)}{G(\frac{\omega_p^2}{\omega_o^2}, \omega_o\tau)} = \frac{PD}{4} (\frac{2\omega_p^2\tau}{\omega_o}) \frac{n}{n} \qquad [52]$$

or

$$V_D = \frac{PD}{4} \frac{2\Delta\sigma}{\omega_o\varepsilon_\ell}.$$

Note that this result is valid for all frequency regions ($\omega_o \gtrless \omega_p$).

Case c) for α_1, $\alpha_2 << 1$. Starting with Eq. [44]

$$\Delta V_D = 2PDQ_E(\alpha_1\delta_1 - \alpha_2\delta_2) \qquad [44]$$

we make analogous replacements as in cases a) and b) to get:

$$\Delta V_D = \frac{PD}{4}\left(\frac{Q_o}{Q_E}\, 8\omega\tau\right) \frac{\Delta n}{n}. \qquad [53]$$

This result is computed for frequency Region I, ($\omega_p < \omega$) which has the best response in this case.

6. COMPARATIVE PERFORMANCE

In order to compare these responses with the photoconductive effect, we compute the increment of voltage at the discriminator under the assumption that the reflection coefficient of the cavity is:

$$\rho = \frac{1 - m^2R_{ob}}{1 + m^2R_{ob}} \qquad [54]$$

Eq. [54] is derived from Eq. [21]. Very low values of Q are used for this case, and the best condition is for critical coupling to the cavity[18]. The discriminator voltage then becomes

$$\Delta V_D = \frac{PD}{4}\,\frac{\Delta n}{n} \qquad [55]$$

Case b), $\alpha = 1$, is shown by Pound to produce the maximum output error voltage from a klystron oscillator stabilized by a cavity. Assuming a Photodielectric Detector and a competing Photoconductive Detector will operate in this mode, we can compare their performance by defining a Performance Factor π as the ratio of Eq. [52] and Eq. [55].

$$\pi = \frac{\Delta V_{PDE}}{\Delta V_{PCE}} = \frac{2\,\omega_p^2\omega_o\tau}{\omega_o^2} \qquad [56a]$$

Since $\sigma_o = ne^2\tau/m^* = \omega_p^2\tau\varepsilon_\ell$, we can rewrite Eq. [56a] in terms of the dielectric time constant $\tau_D = \varepsilon_\ell/\sigma_o$ to get

$$\pi = \frac{2}{\omega_o\tau_D} \qquad [56b]$$

This shows a Photodielectric Detector will be more sensitive than a Photoconductive Detector if $\omega_o\tau_D < 2$. This relation guides the designer in choosing between the P/D detector and P/C detector if the frequency and dielectric time constant of the semiconductor is fixed. The semiconductor would be chosen because of its quantum efficiency at the optical wavelengths to be detected. Its dielectric time constant would be subject to considerable variation by doping.

Sommers, et al.[18,19] has described the performance of the Photoconductive Detector which uses a magic-tee discriminator. It produces the same discriminator voltage, V_D, from a change in reflected power due to a change in the real part of the reflection coefficient. Eqs. [56a] and [56b] provide a means to compare the changes in the real and imaginary components of ρ, given Eq. [21], Chapter I. This puts the Photodielectric Detector in a position to be compared quantitatively with the Photoconductive Detector for Sensitivity.

For the Photodielectric Detector, the change in resonant frequency is greatest in Region II. Taking

$$\Delta f_o = -\frac{g^2}{2\pi C_T}\,\Delta B\left(\frac{\omega_p^2}{\omega_o^2},\ \omega_o\tau_D\right) \qquad [36]$$

and

$$\Delta B\left(\frac{\omega_p^2}{\omega_o^2},\ \omega_o\tau\right) = \omega_o^2\Delta\omega_p^2\omega_o C_o \qquad [57]$$

with Eq. [30]

$$\Delta f_o = - 2\eta f_o \tau^2 \Delta\omega_p^2$$

or also

$$\Delta f_o = - \frac{2\eta f_o \tau}{\epsilon_\ell} \Delta\sigma_o \qquad [58]$$

then

$$\frac{\Delta f_o}{f_o} = - \frac{2\eta\tau\Delta\sigma}{\epsilon_\ell} = - 2\eta\omega_o\tau\left(\frac{\Delta\sigma}{\omega_o\epsilon_\ell}\right). \qquad [59]$$

7. FEEDBACK LOOP

Figure 23 shows a block diagram of the system as described in the introduction, but includes the sources of noise due to the diodes V_{nD} and amplifier V_{nA}.

The frequency of the oscillator source (klystron) f_{osc} is given by Eq. [60]

$$f_{osc} = f_1 + KV_r \qquad [60]$$

where f_1 = the klystron frequency when $V_r = 0$,

V_r = the incremental reflector voltage, and

K = the pushing frequency factor of the klystron.

The output voltage of the amplifier is

$$V_o = -AV_i = - A(V_D' + V_{nA}) \qquad [61]$$

where A is the amplification factor. Calling Eq. [41] the output voltage of the discriminator,

$$V_D' = \frac{DP}{2B_W} \Delta f + V_{nD} \qquad [41]$$

for $\Delta f = f_{osc} - f_o$.

Then, combining Eqs. [60], [61], and 41] together results in the expression for the oscillator frequency of the circuit shown in Figure 23.

$$f_{osc} = \left(\frac{1}{1+H}\right)^2 f_1 + \left(\frac{H}{1+H}\right)^2 f_o - \left(\frac{KA}{1+H}\right)^2 (V_{nD} + V_{nA}) \qquad [62]$$

where $H = \frac{AKDPQ_o}{2f_o}$. [63]

EXAMPLE:

Typical values are: $A = 10^3$

$D = .05$ V/mW

$P = 1$ mW

$Q = 10^3$

$K = 1$ MHz/Volt

$f_o = 10^{10}$ Hz

with these values, $H = 25$.

The maximum frequency shift is for

$$V_D = \frac{PDQ_o}{2f_o} \cdot \left(\frac{\alpha}{1+\alpha}\right)$$

$$\Delta f_{osc}\Big|_{max} = \frac{KAPDQ_o}{2f_o} \cdot \frac{\alpha}{1+\alpha}\Big|_{\alpha=1} = \frac{H}{2} = 12.5 \text{ MHz}.$$

From Eq. [62] the responsivity of the loop system can be computed:

$$\overline{\Delta f}_{osc} = \frac{H}{1+H}\,\overline{\Delta f}_o \qquad [64]$$

8. CIRCUIT NOISE

From Eq. [62] the mean square fluctuation of the klystron frequency $\overline{\Delta f^2_{osc}}$ can be computed as follows:

$$\overline{\Delta f^2_{osc}} = \left(\frac{1}{1+H}\right)^2 \overline{\Delta f^2_o} + \left(\frac{1}{1+H}\right)^2 \overline{\Delta f^2_1} + \left(\frac{\Delta f_o H}{(1+H)^2}\right)^2 \cdot \left[\frac{\overline{\Delta A^2}}{A^2} + \frac{\overline{\Delta P^2}}{P^2} + \frac{\overline{\Delta D^2}}{D^2} + \frac{\overline{\Delta Q_o^2}}{Q_o^2}\right]$$
$$+ \left(\frac{KA}{1+H}\right)^2 \overline{(V^2_{nD} + V^2_{nA})}. \qquad [65]$$

Eq. [65] shows the importance of feedback in the circuit when the value of H is much greater than one:

$$H = \frac{KAPDQ_o}{2f_o} >> 1 \qquad [66]$$

Under this condition the circuit noise is attenuated and Eq. [65] becomes

$$\overline{\Delta f^2_{osc}} \simeq \overline{\Delta f^2_o} + \left(\frac{2B_W}{DP}\right)^2 \cdot (\overline{V^2_{nD}} + \overline{V^2_{nA}}) \qquad [67]$$

where the first part corresponds to the cavity resonant frequency noise from all mechanisms including the sample noise, and the second part is due to the amplifier and diode noise.

9. DETERMINATION OF THE OPERATING FREQUENCY FOR THE PDE

From Eq. [62] we find

$$\overline{\Delta f_{osc}} \simeq \frac{H}{1 + H}\,\overline{\Delta f_o} \qquad [68]$$

for

$$\overline{\Delta f_1} = \overline{V}_{nD} = \overline{V}_{nA} = 0$$

and the measured value of f_{osc} is within the limits:

$$\overline{\Delta f_{osc}} = \overline{\Delta f_o} \pm (\overline{\Delta f^2_{osc}})^{1/2} \qquad [69]$$

where $\overline{\Delta f^2_{osc}}$ is taken from Eq. [67]

$$\overline{\Delta f^2_{osc}} = \overline{\Delta f^2_o} + \left(\frac{2B_W}{DP}\right)^2 \cdot (\overline{V^2_{nD}} + \overline{V^2_{nA}}). \qquad [70]$$

This implies that

$$\frac{1}{H^2}\,\overline{\Delta f^2_1} << \overline{\Delta f^2_o} \qquad [71]$$

which defines the value required for H so the noise from the source can be neglected.

For the detectivity to be limited by the sample noise, $\overline{\Delta f_o^2}$, and not by diode and amplifier noise, the following relation has to be true:

$$\overline{\Delta f_o^2} > \left(\frac{2B_W}{DP}\right)^2 \cdot (\overline{V_{nD}^2} + \overline{V_{nA}^2})$$

or

$$\overline{\Delta V_D^2} = \left(\frac{DP}{2B_W}\right)^2 \overline{\Delta f_o^2} > (\overline{V_{nD}^2} + \overline{V_{nA}^2}) \qquad [72]$$

Substituting Eq. [52] into [69] we have:

$$\left(\frac{DP}{2} \frac{\omega^2 \tau}{\omega N}\right) \cdot \overline{\Delta N^2} > \overline{V_{nD}^2} + \overline{V_{nA}^2} \qquad [73]$$

where N and ΔN are number of free carriers.

If we assume that the diodes and amplifiers are limited by thermal noise then

$$\overline{V_{nD}^2} + \overline{V_{nA}^2} = 2KTR_L B_W \qquad [74]$$

where K = the Boltzman's constant

T = absolute temperature of the diodes and amplifiers.

R_L = resistance, diode and input of the amplifier.

B_W = bandwidth.

$\overline{\Delta N^2}$ is computed assuming that it originates from gaussian or thermal fluctuations, then it becomes[20]

$$\overline{\Delta N^2} = \overline{(\Delta N - \overline{\Delta N})^2} = \overline{N^2} - \overline{N}^2 = \overline{N} \qquad [75]$$

Using Eqs. [71] and [72] in Eq. [70] we have

$$\left(\frac{DP}{\omega}\right)^2 \cdot \frac{1}{B_W} > \frac{2KTR_L V_s}{n} \cdot \left(\frac{2m^* \epsilon_\ell}{e^2 \tau}\right) \qquad [76]$$

where V_s is the sample volume.

If the inequality, Eq. [76], is true, then the output noise due to the diodes and amplifier is negligible compared to the sample thermal noise. This latter component is the dark current noise. For example, we compute

the inequality, Eq. [76], for the following typical values:

For the Sample: $n = 10^{12}$ elect./cm^3,

$V_s = 10^{-2} cm^3$,

$\tau = 10^{-10}$ sec,

$\varepsilon_\ell = 10\ \varepsilon_o$,

$m^* = m_o$;

For the diodes and amplifier: $R_L = 200\ \Omega$

$T = 300°K.$

Then with these values we have

$$(\frac{DP}{\omega})^2 \frac{1}{B_W} > .68 \times 10^{-30} \text{Volt}^2 \text{sec}^3. \qquad [77]$$

Inequality, Eq. [77], indicates the maximum value of the cavity resonant frequency ω for the different values of the bandwidth B_W, diode efficiencies D, and the source microwave power P.

The maximum allowed value of P is such that the average distance travelled by the free carrier in a period is less than the length of the sample. From Eq. [2], the maximum distance travelled by the free carrier is at a frequency equal to the plasma frequency. For this case, the relation between the maximum power P_{max} and the sample length is

$$P_{max} = \frac{nV_s m^* \omega^2 \ell^2}{\tau} \qquad [78]$$

for $n = 10^{12}$ elect./cm^3,

$V_s = 10^{-2}\ cm^3$,

$m^* = m_o$,

$\tau = 10^{-10}$ sec.

then $P = 10^{-10}\ \omega^2 \ell^2$,

and for ℓ in mm and P in mW

$$P_{max}(mW) = 10^{-13}\omega^2\ell^2(mm) \qquad [79]$$

Using Eq. [79] into [77] and for ℓ = 1 mm

$$\frac{1}{B_W} = \left(\frac{D \times 10^{-13} \times \omega^2 \times \ell^2}{\omega}\right)^2 \frac{1}{B_W} > .68 \times 10^{-30}\,\text{Volt}^2\text{sec}^3$$

$$\frac{D^2\omega^2}{B_W} > .68 \times 10^{-4}\,\text{Volt}^2\text{sec}^3 \qquad [80]$$

where D is in Volt/mW.

Typical values of D are of order of unity then

$$\frac{\omega^2}{B_W} > .68 \times 10^{-4}\,\text{sec}^{-1}. \qquad [81]$$

This shows that higher frequencies have better performances if, and only if, the power can be increased up to P_{max}. The value of P_{max} can be computed from Eqs. [78] and [79].

10. BANDWIDTH OF THE CAVITY

To measure the resonant frequency of the cavity, the response has to relax to its steady state, which happens when the transient state is over. The decay constant is τ_C,

$$\tau_C = \frac{Q}{\omega_o}$$

and the bandwidth is defined by

$$B_W = \frac{f_o}{Q} = \frac{1}{2\pi\tau_C}. \qquad [82]$$

Under the condition that the cavity Q is mainly dominated by the sample, from Eq. [46] we have

$$Q = \omega_o R_T C_T = \frac{\omega_o C_T}{g^2 G\left(\frac{\omega_p}{\omega_o}, \omega_o\tau\right)} \qquad [83]$$

From Eq. [32] can be chosen three frequency regions to compute $G(\omega_p^2/\omega_o^2, \omega_o\tau)$,

REGION I: $\omega_p < \omega_o$ and $\omega_o\tau > 1$

$$G(\frac{\omega_p^2}{\omega^2}, \omega_o\tau) \simeq \omega_o C_o (\frac{\omega_p^2}{\omega_o^2}) \frac{1}{\omega_o\tau} \quad [84]$$

REGION II: $\omega_p \simeq \omega_o$

$$G(\frac{\omega_p^2}{\omega_o^2}, \omega_o\tau) \simeq \omega_o C_o (\frac{\omega_p^2}{\omega_o^2}) \omega_o\tau \quad [85]$$

REGION III: $\omega_p > \omega_o$ and $\omega_o\tau > 1$

$$G(\frac{\omega_p^2}{\omega^2}, \omega_o\tau) \simeq \omega_o C_o (\frac{\omega_o^2}{\omega_p^2}) \frac{1}{\omega_o\tau} \quad [86]$$

with Eqs. [84], [85], [86] and [30] in Eq. [83], we have the different values of Q for

REGION I: $$Q_I \simeq \frac{\omega_o\tau}{2\eta} (\frac{\omega_o^2}{\omega_p^2}) \quad [87]$$

REGION II: $$Q_{II} \simeq \frac{1}{2\eta\omega_o\tau} (\frac{\omega_o^2}{\omega_p^2}) \quad [88]$$

REGION III: $$Q_{III} \simeq \frac{\omega_o\tau}{2\eta} (\frac{\omega_p^2}{\omega^2}) \quad [89]$$

11. OTHER ADVANTAGES OF THE PDE

The PDE also has all the advantages of RF bias techniques. These are the following:

First: No ohmic contacts are required as is the case for DC Photoconductivity. For photoconductivity carriers collected by one contact must be replenished by the other, or injected into the bulk in order to maintain charge neutrality.

Second: The RF or microwave field is applied at a frequency sufficiently high that carriers travel slightly less than the width of the

sample during one half of the RF cycle. The photocarrier is then effectively trapped in the bulk of the material and it shuttles back and forth until bulk recombination occurs. This increases the effective lifetime.

Third: If the AC field is capacitatively coupled, the sample dimensions can be made minute, and hence the gain can be high, because space charge injection does not become important. The transformation of the high impedance of the sample to low impedance of the following amplifier allows the sensitivity to be maintained over a broad bandwidth (i.e., in Eq. [74]) $R_L \simeq 200\ \Omega$. This allows the use of high purity samples.

Fourth: The gain in both cases depends on the voltage applied to the semiconductor. An AC field allows higher voltages for the same displacement of the free carriers. This displacement is smaller than the sample width to avoid carrier sweep-out. This means that the gain for PDE and PC is proportional to the frequency.

12. OTHER SYSTEMS SUGGESTED TO MEASURE THE PDE

There are different methods that have been suggested[21] to measure the change in the resonant frequency of the cavity loaded with a semiconductor. All of these methods can be summarized into two types. The former use the cavity as a part of a linear circuit. In the circuit there is a reference source which applies a signal to the cavity and the cavity output is compared with the input. From this comparison is determined the change in cavity resonant frequency.

The comparison can be made in many ways: power of the reflected wave, power of the transmitted wave and phase difference between the output and

input. All of these ways are related and have analogous results to the system analyzed in Chapter II of the present work. The transient and steady state analysis of these types of systems are easy to analize and the results are computed without difficulties.

The latter method uses the cavity as a part of a non-linear system. An example is an oscillator built with a transmission cavity and a traveling wave amplifier. The transient response of this system is difficult to analyze, but the operating conditions under steady state are easy to determine. The frequency change of the oscillator is also proportional to $Q\delta$ as was discussed for the former type of system. An oscillator using a klystron loaded by the cavity is another example of this class[22]. The change in the impedance of the cavity due to a change in the sample will cause a change in the frequency of the klystron proportional to the pulling factor. In this case, the change in frequency is also proportional to the change of the product $Q\delta$, which represents the susceptance of the cavity.

CHAPTER III.

THE SAMPLE AS A PHOTODETECTOR

1. INTRODUCTION

For a general photodetector there are three major processes: (1) Carrier generation by incident light; (2) carrier transport and/or multiplication by whatever current gain mechanism may be present; and (3) interaction of current with external circuitry to provide the output signal.

In Chapters I and II points (2) and (3) above, are treated in classical terms. A lumped model was developed, and the difference between the PDE and PC was established. We saw that the PDE provides a different way to measure the variation of free carrier density in a semiconductor. We have also defined Performance Factor (Eq. [56]) which is the ratio between the PDE and PC responses.

This chapter deals with point (1) mentioned above, corresponding to the interaction between the radiation to be detected and the sample material used as a detector. This interaction is similar in all solid state photodetectors, for which it is convenient to write a summary on the extensive work done in this area. The conclusions of this summary, especially related to photoconductivity, will be extrapolated to the case of the PDE through the Performance Factor (Eq. [56]). This is done in order to calculate the different quality parameters for the PD detector.

The generation of carriers by incident light is governed by the maintenance of a non-equilibrium carrier distribution through a dynamic balance of the generation and recombination processes. The sensitivity is related directly to the non-equilibrium carrier density which can be established by optical absorption. The speed of response depends on the kinetics of

new non-equilibrium situations responding to changes in the level of optical excitation.

Various summaries are available on photodetector theory. They compare the different types of photodetectors and give expressions for the appropriate parameters for each type. Of greatest interest to us are those on solid state photodetectors[23-28] and especially AC photoconductors[18,19] because they have the photon bulk absorption and the transport processes in common with the PDE.

Four different models are generally developed to explain the photoelectrical properties of (bulk) solid state semiconductor photodetectors. These models represent different energy levels for the electrons, conduction and valence band, and traps and recombination centers[25]. In general, the equations that represent these models are coupled non-linear differential equations. Steady state solution can be found using various approximations.

The brief summary on photodetectors covers: generation and recombination of free carriers, spectral and frequency responsivity, and noise for different materials used as PDE detectors. The chapter includes a discussion on improving photodielectric response.

2. GENERATION AND RECOMBINATION

Using the simplest model in which the detection process is determined by one type of carrier only (i.e., the other type of carrier recombining very rapidly), the rate equation of the electron density n has the following form:

$$\frac{dn}{dt} = ge^{j2\pi f_m t} - \frac{n}{\tau_L} \qquad [90]$$

where $ge^{j2\pi f_m t}$ is the generation rate of electrons per unit detector area A given by

$$g = \eta(\nu) \frac{P_o}{Ah\nu} \qquad [91]$$

$\eta(\nu)$ is the quantum efficiency coefficient. It is defined as the ratio of carriers detected to incident photons. Figure 24 shows a qualitative dependence[24] of $\eta(\nu)$ versus the photon energy as function of the bulk light absorption coefficient α and the surface recombination. P_o is the power of the incident light on the surface of the detector. Its values vary as

$$P(x) \sim P_o e^{-\alpha x} \qquad [92]$$

where α = the bulk absorption coefficient,

$h\nu$ = the photon energy of the incident photons,

f_m = the frequency of the modulated signal.

The steady state solution for Eq. [90] is

$$n(f_m) = \frac{g\tau_L}{[1 + (2\pi f_m \tau_L)^2]^{1/2}} \qquad [93]$$

where τ_L is the lifetime of the free carriers.

The last equation influences the frequency response of the photodetector. For

$$f_m < \frac{1}{2\pi\tau_L} \qquad n(f_m) = g\tau_L \qquad [94a]$$

and for

$$f_m > \frac{1}{2\pi\tau_L} \qquad n(f_m) = \frac{g}{2\pi f} \qquad [94b]$$

The bandwidth of the sample is defined by

$$B_s = \frac{1}{2\pi\tau_L} \qquad [95]$$

From Eq. [94a] we note that the response is directly proportional to τ_L. From Eq. [92] the bandwidth is inversely proportional to τ_L.

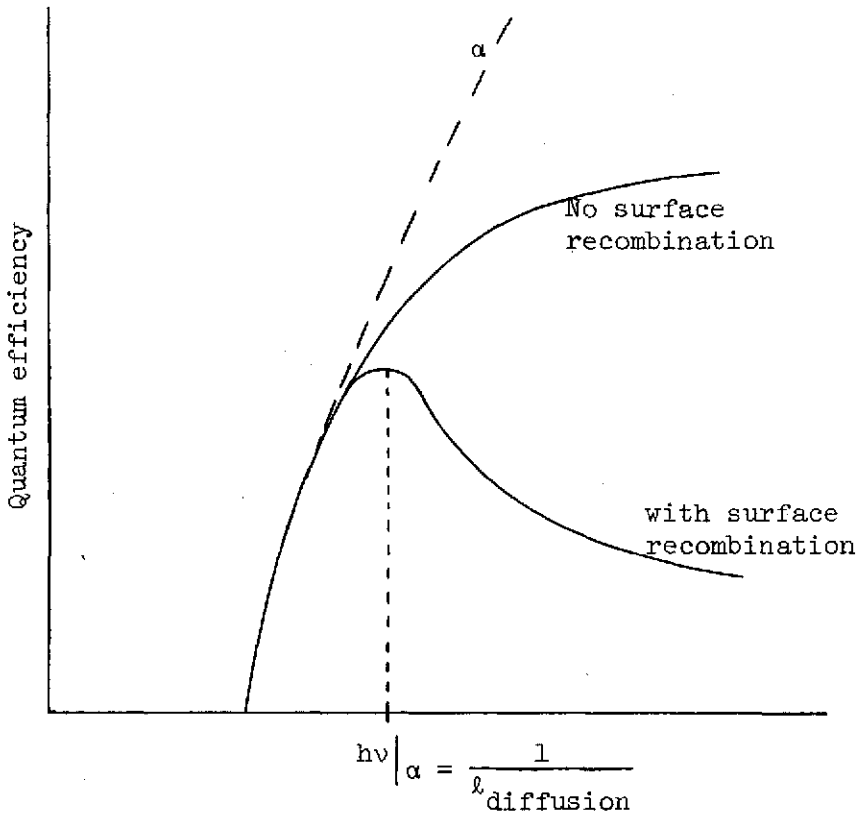

FIGURE 24. Qualitative dependence of quantum efficiency on photon energy.

3. NOISE IN PHOTODETECTORS:

The sources of noise are classified[25], depending on the location of the source:

1. Noise produced by the blackbody photon field.
2. Noise produced by the ambient photon field.
3. Noise associated with the signal.
4. Spontaneous noise characteristic of the device, but not associated with 2, above.
5. Noise associated with the circuitry and amplifiers.

The three former sources are external to the detector and are common to all photodetectors. Under ideal circumstances, these can be neglected leaving only the two latter sources which determine the quality of different photodetectors and allows their comparison.

From the detector point of view it is more useful to distinguish the (spontaneous) noise of the device in different physical process, the most important are:

1. Thermal noise,
2. generation-recombination noise,
3. transport noise (diffusion and drift, especially shot noise),
4. excess noise (1/f, temperature, surface imperfections).

The total noise voltage $N_T(f_m)$ at the output of the detector is:

$$N_T(f_m) = [S_{det}(f_m) + S_{eq}(f_m)]^{1/2} B_W^{1/2} \qquad [96]$$

where $S_{det}(f_m)$ is the frequency density fluctuation noise associated with the detector and $S_{eq}(f_m)$ is the equivalent frequency density fluctuation due to the external circuit.

The incident signal to be detected is represented by $j(\nu, f_m)$ which is the number of photons per second incident on the total detector area A,

$$j(\nu, f_m) = \frac{P(f_m)}{h\nu A} \qquad [97]$$

where ν and f_m represent the spectral and modulation frequencies, respectively.

The output response of the detector is represented by $r(f_m)$. Then the responsivity of the detector is defined as $R(\nu, f_m)$ such that:

$$r(f_m) = R(\nu, f_m)\, j(\nu, f_m). \qquad [98]$$

The power signal noise ratio SNR is

$$SNR = \left(\frac{r(f_m)}{N_T(f_m)}\right)^2 = \frac{j^2(\nu, f_m)R^2(\nu, f_m)}{[S_{det}(f_m) + S_{eq}(f_m)]\, B_W} \qquad [99]$$

The spectral apparent noise equivalent power (spectral ANEP) is defined as the input signal J'_{eq} for SNR = 1, thus:

$$P'_{eq}[\nu, f_m, B_W, A] = h\nu_s J'_{eq}[\nu, f_m, B_W, A] =$$

$$\frac{h\nu[S_{det}(f_m) + S_{eq}(f_m)]^{1/2}(B_W)^{1/2}}{R(\nu, f_m)} \qquad [100]$$

The quantities in the brackets indicate that P'_{eq} depends upon the optical frequency $\nu = c/\lambda$, the modulation frequency f_m, the bandwidth of the detector B_W, and the detector area A.

Similarly, we introduce the spectral real noise equivalent power (spectral RNEP) defined as:

$$P_{eq}[\lambda, f_m, B_W, A] = \frac{h\nu[S_{det}(f_m)\, B_W]^{1/2}}{R(\nu, f_m)} \qquad [101]$$

The spectral RNEP holds for the detectors in which the noise does not depend on the external electronic circuit (i.e., $S_{eq}(f_m) << S_{det}(f_m)$. This type of detector is called "Class A" by Jones[30]. Those that behave as Eq. [100], in which the noise depends on the external circuit, are called "Class B" detectors. No figure of merit can be given for these detectors unless special reference conditions are defined.

In Chapter II, Section 9 are defined the operating conditions under which the circuit noise is minimized and the detectivity is limited by the sample noise. This classifies the photodielectric detector among the various types of Class A detectors.

The spectral specific noise equivalent power (spectral SNEP) is obtained when the bandwidth $B_W = 1$ Hz, and when the area of the detector $A = 1$ cm^2. It is denoted by $P_{eq}[\lambda, f_m, 1, 1]$. For most detectors the rms noise is proportional to the square root of the area. Hence in an ideal case

$$P_{eq}[\lambda, f_m, B_W, A] = P_{eq}[\lambda, f_m, 1, 1]\ (AB_W)^{1/2} \qquad [102]$$

The <u>detectivity</u> is defined as the reciprocal of the noise equivalent power, so that the spectral detectivity D* is the reciprocal of the spectral SNEP.

$$D^* = D[\lambda, f_m, 1, 1] = \frac{1}{P_{eq}[\lambda, f_m, 1, 1]} = D^*[\lambda, f_m]. \qquad [103]$$

The units of D* are cm $\sec^{-1/2}W^{-1}$.

It is difficult to summarize the sample noise mechanisms in various materials, since they are widely different. Reference 25 expresses the change in electron and hole densities in solid state bulk photodetectors. These are done for four different ideal models in which generation-recombination noise is considered as the limiting noise.

In order to compute the detectivity for the PDE we define the response $r(f_m)$ as the output of the discriminator given by

$$r(f_m) = V_D = \frac{PD}{2}\left(\frac{e^2\tau}{m^*\omega\varepsilon_\ell V_s}\right)\Delta N(f_m) \qquad [104]$$

where f_m is the light modulation frequency, and $\Delta N(f_m)$ is the change in number of electrons generated by the optical signal.

For the conditions given in Sections 8 and 9 of Chapter II, the output noise is due mainly to the fluctuations of free carriers in the sample, $\overline{\Delta N^2(f_m)}$. Then

$$N_T(f_m) = \frac{PD}{2}\left(\frac{e^2\tau}{m^*\omega\varepsilon_\ell V_s}\right)\left(\overline{\Delta N^2(f_m)}\right)^{1/2} \qquad [105]$$

with the Eqs. [104] and [105] in Eq. [99], we compute the SNR for the PDE

$$SNR = \left(\frac{r(f_m)}{N_T(f_m)}\right)^2 = \frac{\overline{\Delta N(f_m)}^2}{\overline{\Delta N^2(f_m)}} . \qquad [106]$$

$\Delta N(f_m)$ is due to the change in signal Power, and it can be expressed in terms of a spectral responsivity for electrons, $R^N(\nu, f_m)$,

$$\Delta N(f_m) = R^N(\nu, f_m)\, j(\nu, f_m). \qquad [107]$$

Recalling Eq. [93], $\Delta N(f_m)$ becomes

$$\Delta N(f_m) = \ell A\eta = \frac{\ell A g \tau_L}{[1 + (2\pi f_m \tau_L)^2]^{1/2}} \qquad [108]$$

where ℓ is the effective thickness of the sample. This is considered to be of the same order as the penetration depth.

With Eq. [91] for g and Eq. [97] in Eq. [108] we have

$$\Delta N(f_m) = \eta(\nu)\ell A \left[\frac{\tau_L}{[1 + (2\pi f_m \tau_L)^2]^{1/2}}\right] j(\nu, f_m) \qquad [109]$$

then

$$R^{(N)}(\nu, f_m) = \ell A \eta(\nu) \cdot \left[\frac{\tau_L}{[1 + (2\pi f_m \tau_L)^2]^{1/2}} \right] \qquad [110]$$

$\overline{\Delta N^2(f_m)}$ is due to free carrier fluctuations in the sample and it is expressed by

$$\overline{\Delta N^2(f_m)} = S^N(f_m) B_W$$

where $S^N(f_m)$ is the frequency density fluctuation of electrons and B_W is the bandwidth of the detector.

$S^N(f_m)$ is computed[32] for an extrinsic type of sample, assuming generation-recombination noise. The final result is

$$S^{(N)}(f_m) = 4nA\ell \cdot \left[\frac{\tau_L}{1 + (2\pi f_m \tau_L)} \right]. \qquad [111]$$

Similarly, for a near-intrinsic type of sample we have

$$S^{(N)}(f_m) = 4\left(\frac{np}{n+p}\right) A\ell \cdot \left[\frac{\tau_L}{1 + (2\pi f_m \tau_L)^2} \right] \qquad [112]$$

For the extrinsic case, with Eq. [109] and Eq. [111] into Eq. [105], we have the final expression for SNR

$$SNR = \frac{\eta^2(\nu) \tau_L P}{4nA\ell B_W}. \qquad [113]$$

For $A = 1\ cm^2$, $B_W = 1$ Hz and SNR = 1, the specific detectivity D* for the extrinsic sample is

$$D^*(\text{extrinsic}) = \frac{\eta(\nu)}{2h\nu} \left(\frac{\tau_L}{n\ell}\right)^{1/2}. \qquad [114]$$

Similarly for the near-intrinsic type[25]

$$S^{(N)} \simeq \frac{4np}{n+p} (A\ell) \cdot \left[\frac{\tau_L}{1 + 2\pi f_m \tau_L} \right] \qquad [115]$$

which gives the final result for D*

$$D^*(\text{intrinsic}) = \frac{\eta(\nu)}{2h\nu}\left[\frac{n+p}{np}\cdot\frac{\tau_L}{\ell}\right]^{1/2} \qquad [116]$$

4. EXPERIMENTAL EXAMPLES

In previous experiments on the PDE carried out by Arndt[3] and Stone[1] with high purity samples of p-type germanium and silicon, specific detectivity as high as 3×10^{13} cm cps$^{1/2}$/Watt were found. Also, a change in the cavity resonant frequency of 15 KHz per milliwatt was measured. The experiment uses a cavity at 910 MHz, a GaAs light source (9000 Å), a filling factor $\eta = 0.02$, a relaxation time $\tau = 10^{-10}$ sec, a lifetime $\tau_L = 10^{-7}$ sec, and a sample volume $V_s = 10^{-2}$ cm^3. Using these values in the model of the present work (Eq. [58]), a responsivity of 46 MHz per mW is possible, three orders higher than the value observed in the experiment. This theoretical performance can be achieved by observing the following conditions:

1. A higher resistivity sample would produce a lower electron density in the dark. This decreases the noise equivalent power.
2. Materials with high quantum efficiency at 9000 Å could be used.
3. The highest change in resonant frequency would have been obtained at a cavity frequency equal to the plasma frequency of the sample.
4. The low cavity Q was due to the effective sample losses (i.e., losses of the free electron generated by the incident light) in a sample larger than necessary to absorb all the light.
5. The loaded cavity should be coupled to the waveguide at the critical coupling condition.
6. The surface recombination has to be minimized by etching the surface. (This reduces surface imperfection).

From data by Kung[31] on 7.4 Ω-cm p-type silicon, shown in Figure 25, the computed performance gave $\omega\tau = 2.74$ at 4.2°K and at a frequency of 960 MHz. This sample had $\omega_p^2 \simeq \omega^2$, giving the Performance Factor, $\pi = 5.58$. While this performance could have been improved by observing the conditions cited above, this photodielectric detector was 5.58 times as sensitive as an AC photoconductive detector in the same circuit.

The sample used by Kung had a filling factor of 0.02 from cavity frequency-shift measurements. From Eq. [58] a value of $\eta = 0.0003$ is calculated, meaning the useful volume of the sample is $\sim$ 67 times less than the actual volume, due to the large photon absorption coefficient for silicon at 9000 Å. An improvement in detector performance of this much can be expected if the sample size was reduced.

Experiments by Johnson[33] on InSb at 2.33 GHz, 4.2°K gave an $\omega\tau = 3.86$ and $\omega_p^2 \simeq 0.8\omega^2$. This photodielectric detector is 6.2 times as sensitive as the same system in the AC photoconductive mode as predicted by the Performance Factor, π.

From these examples, it is evident that photodielectric detectors can produce a greater output signal than an AC-biased photoconductor, and that the performance previously reported could have been significantly improved with appropriate choice of materials and cavity frequency.

In retrospect, the AC photoconductive detector measures the real part of the reflected power from the cavity. The photodielectric detector measures the imaginary component of the reflected power. If the semiconductor parameters are properly chosen, the SNR and detectivity of the PD detector will be superior. The bandwidth will be the same in each case for a given sample in the same cavity. A significant advantage is the absence of ohmic

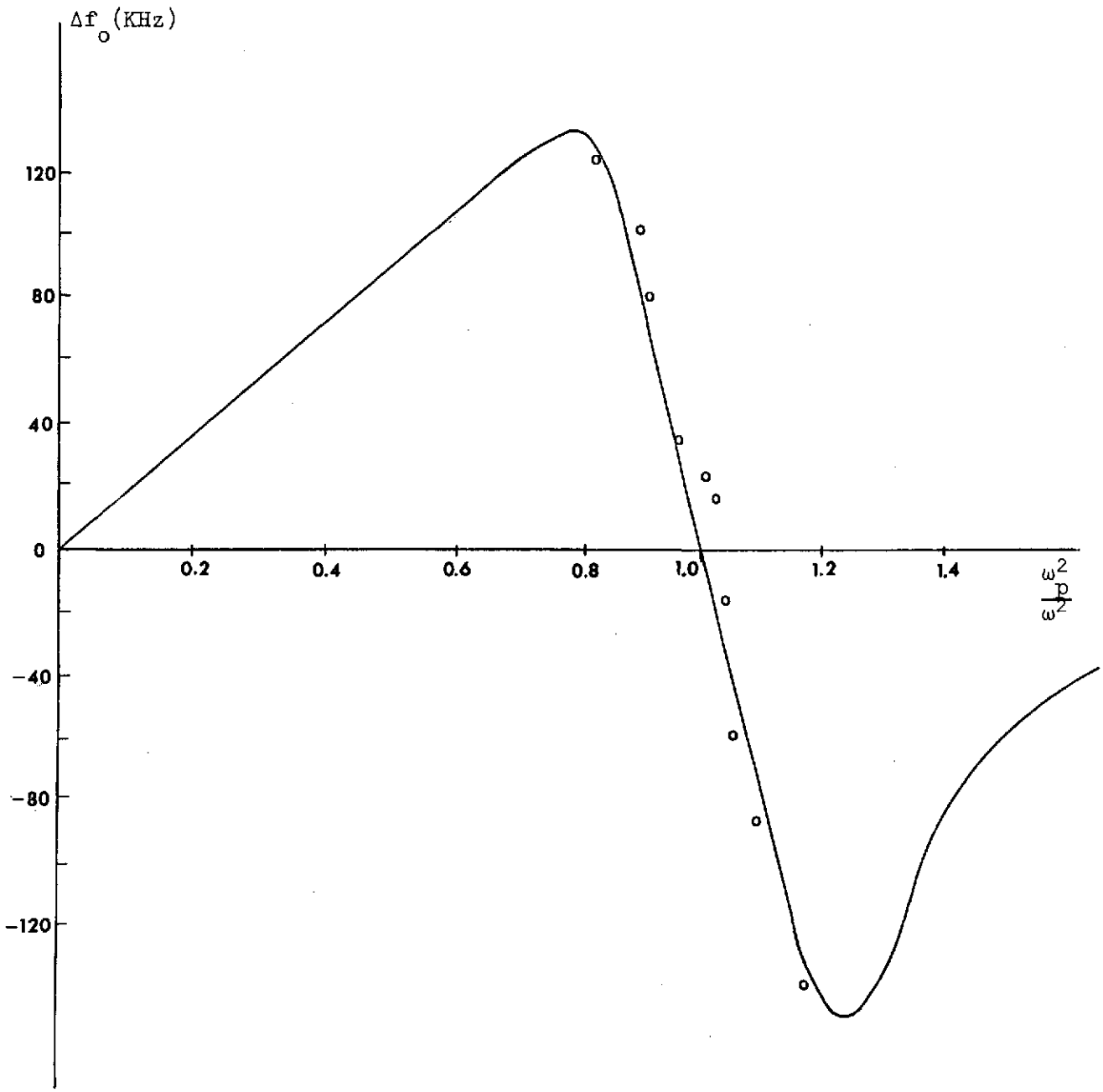

FIGURE 25. Frequency shift vs. ω_p^2/ω_o^2 for 7.4 Ω-cm p-type Si(undoped), $\omega\tau = 2.79$, $T = 4.2^\circ K$, $\lambda = 9000$ Å and $f_o = 860$ MHz.

contacts on the PD sample, which increases the variety of materials which can be used. This, in turn, widens the choice of wavelengths which can be detected, since ohmic contacts are virtually unattainable on dielectric materials at low temperature. The value of D* is a function of the sample parameters at a particular wavelength. As such it has the same value for PD and PC detectors.

5. CONCLUSIONS

The photodielectric detector is shown to be equal to superior to an AC photoconductive detector using the same sample, frequency, temperature and external circuitry. The Performance Factor, $\pi \equiv 2/\omega_o \tau_D$, (see p. 45), is the numerical ratio of sensitivities. Since the cavity resonant frequency, ω_o, and the dielectric time-constant of the sample, τ_D, are controlled by the system design and choice of semiconductor, the performance factor can be greater than unity. The performance parameters derived in this report can be directly compared with any photodetector which can be compared to an AC photoconductor.

Thus, the research conducted under this grant has successfully demonstrated the photodielectric detector deserves a place among all the best ways to receive optical and infrared signals.

APPENDIX A

ELECTRON HOLE DYNAMIC EFFECTS WITH A STATIC MAGNETIC FIELD

Following the argument of section 3, Chapter I, for the case when two types of carriers, are present in the semiconductor, Eq. [A1] is the equation of motion for the particles. The particles are coupled by forces originated from their restoring or depolarization fields.

$$\ddot{x}_1 + \frac{1}{\tau_1}\dot{x}_1 + \omega_{p_{x1}}^2 x_1 + \omega_{p_{x2}} x_2 = \frac{e_1}{m_1^*} E - \frac{e_1 B_z}{m_1^*} \dot{y}_1$$

$$\ddot{y}_1 + \frac{1}{\tau_1}\dot{y}_1 + \omega_{p_{y1}}^2 y_1 + \omega_{p_{y2}} y_2 = \frac{e_1 B_z}{m_1^*} \dot{x}_1$$

$$\ddot{x}_2 + \frac{1}{\tau_2}\dot{x}_2 + \omega_{p_{x2}}^2 x_2 + \omega_{p_{x1}}^2 x_1 = - \frac{e_2}{m_2^*} E - \frac{e_2 B_z}{m_2^*} \dot{y}_2$$

$$\ddot{y}_2 + \frac{1}{\tau_2}\dot{y}_2 + \omega_{p_{y2}}^2 y_2 + \omega_{p_{y1}}^2 y_1 = \frac{e_2 B_z}{m_2^*} x_2 \qquad [A.1]$$

The fourth term in the first part of each equation in Eq. [A.1] represent a coupling term.

APPENDIX B.

FREE, BOUND AND TRAPPED ELECTRON DYNAMICS IN AN RF ELECTRIC FIELD

These cases involve an equation of motion for each particle. In each equation there is present a coupling term due to each particle. This is represented by Eq. [B1].

$$\ddot{x}_1 + \frac{\dot{x}_1}{\tau_1} + \omega_{p1}^2 x_1 + \omega_{p2}^2 x_2 + \omega_{p3}^2 x_3 + \omega_{p4}^2 x_4 = \frac{e_1}{m_1^*} E$$

$$\ddot{x}_2 + \frac{\dot{x}_2}{\tau_2} + \omega_{p2}^2 x_2 + \omega_{p3}^2 x_3 + \omega_{p4}^2 x_4 + \omega_{p1}^2 x_1 = \frac{e_2}{m^*} E$$

$$\ddot{x}_3 + \frac{\dot{x}_3}{\tau_3} + \omega_{o3}^2 x_3 + \omega_{p4}^2 x_4 + \omega_{p1}^2 x_1 + \omega_{p2}^2 x_2 = - \frac{e_2}{m_3^*} E$$

$$\ddot{x}_4 + \frac{\dot{x}_4}{\tau_4} + \omega_{04}^2 x_4 + \omega_{p1}^2 x_1 + \omega_{p2}^2 x_2 + \omega_{p3}^2 x_3 = - \frac{e_2}{m_4^*} E \qquad [B1]$$

when the sub-indices are:

1 for free electrons,

2 for holes,

3 for shallow electrons,

4 for bound electrons,

the plasma frequencies are

$$\omega_{pi}^2 = \frac{n_i e^2}{m_i^* \varepsilon_o} \qquad \text{for } i = 1,3$$

ω_{oi}^2 does not depend on the density of carriers n_i, but on the atomic binding energy of each particle.

BIBLIOGRAPHY

1. Stone, J.L., W.H. Hartwig, and G.L. Baker, "Automatic Tuning of Superconductive Cavaties Using Optical Feedback," J. App. Phys., 40, No. 5, pp. 2015-2020, April 1969.

2. Hinds, J. and W.H. Hartwig, "Use of Superconductor Cavaties to Resolve Carriers Trapping Effects in CdS," J. of App. Phys., 40, No. 5, pp. 2020-2027, April 1969.

3. Arndt, G.D., J.L. Stone and W.H. Hartwig, "Photodielectric Detector Using Superconducting Cavity," J. of App. Phys., 39, No. 6, pp. 2653-2658, May 1968.

4. Dresselhaus, G., A.F. Kip and C. Kittel, "Cyclotron Resonance of Electrons and Holes in Silicon and Germanium Crystals," Phys. Rev., 98, No. 2, pp. 368-384, April 15, 1955.

5. Michel, R.E., and B. Rosenblum, "Magnetoplasma Resonance in Germanium ," Phys. Rev. 128, No. 4, pp. 1646-1656, Nov. 15, 1962.

6. Wang, S., Solid State Electronics, Chapter 7, McGraw Hill, 1966.

7. Kittel, C., Introduction to Solid State Physics, Chapter 12, John Wiley, 1966.

8. Seitz, F., The Modern Theory of Solids, Chapter 17, McGraw Hill, 1940.

9. Wang, S., Solid State Electronics, p. 395, McGraw Hill, 1966.

10. Pratt, W.K., Laser Communication Systems, Chapter 5, John Wiley, 1969.

11. Ramo, Simon, John R. Whinnery and Theodore Van Duzer, Fields and Wave Communication Electronics, p. 565, John Wiley, 1967.

12. Ginzton, Edward L., Microwave Measurement, pp. 86-91, McGraw Hill, 1957.

13. Ramo, Simon, John R. Whinnery and Theodore Van Duzer, Fields and Wave Communication Electronics, pp. 548-551, John Wiley, 1967.

14. River, Edouard and Mylene Verge-Lapisardi, "Lumped Parameters of a Reentering Cylindrical Cavity," IEEE Trans. on Microwave Theory and Techniques. 19, No. 3, pp. 309-314, March 1971.

15. Baker, G.L. and W.H. Hartwig, "Calculation of Free Carrier Photodielectric Parameters," p. 15, Nasa Technical report, May 1969.

16. Applied Dynamics, AD/4 Reference Manual, Applied Dynamics, Sept. 1967.

17. Pound, R.V., "Frequency Stabilization of Microwave Oscillator," Proc. IRE, 35, pp. 1405-1415, 1947.

18. Sun, C., T.E. Walsh, "Performance of Broad-Band Microwave-Biased Extrinsic Photoconductive Detectors at 10.6μ," IEEE J. of Quant. Elect., 6, No. 7, pp. 450-457, July 1970.

19. Sommers, H.S., Jr. and E.K. Gatchell, "Demodulation of Low Level Broad-Bank Optical Signals with Semiconductors," Proc. IEEE, 54, No. 11, pp. 1553-1568, Nov. 1966.

20. Kittel, C., Elementary Statistical Physics, Part 2, Section 25, John Wiley, 1958.

21. Baker, G.L., W.H. Hartwig, "Calculation of Free Carrier Photodielectric Parameters," Nasa Technical Report, May 31, 1969.

22. Goldstein, I., "Frequency Stabilization of a Microwave Oscillator with an External Cavity," IRE Trans. MTT5, No. 1, January 1971.

23. Melchor, Hans, Mehlon B. Fisher, Frank R. Arams, "Photodetectors for Optical Systems," Proceedings of the IEEE, Vol. 58, No. 10, pp. 1455-1485, Oct. 1970.

24. Anderson L.K., M. DiDomenico and M.B. Fisher, "High Speed Photodetectors for Microwave Demodulation Light," Advances in Microwaves, Academic Press, N.Y. 1970.

25. Van Vliet, K.M., "Noise Limitations in Solid State Photodetectors," Applied Optics, 6, No. 7, pp. 1145-1169, July 1967.

26. Ross, Monte, Laser Receivers, John Wiley, N.Y. 1967.

27. Kruse, Paul W., Laurence D. McGlauchlin, Element of Infrared Technology, John Wiley, N.Y. 1962.

28. Hudson, Richard D., Infrared System Engineering, Wiley Interscience, N.Y. 1969.

29. DiDomenico, M. and L.K. Anderson, "Microwave Signal-to-Noise Performance of CdSe Bulk Photoconductive Detectors," Proceedings of the IEEE, Vol. 52, pp. 815-822, July 1964.

30. Jones, R. Clark, Advances in Electronics, Academic Press, New York, 1953, Vol. 5, pp. 1-96.

31. Kung, Hsing-Hsien, "Use of Photodielectric Response to Observe Effects of Copper on Recombination Lifetime in Silicon at Very Low Temperature," Unpublished, Master Thesis in Electrical Engineering, The University of Texas at Austin, May 1969.

32. Van Vliet, K.M., and J.R. Fassett, Fluctuation Phenomena in Solids, Chapter VII, R.E. Burgess, Ed., Academic Press, New York, 1965.

33. Johnson, J.B., "The Measurement of the Photodielectric Effect in Indium Antimonide Using High Energy Photons," unpublished, Master Thesis in Electrical Engineering, The University of Texas at Austin, May, 1972.